GRADUATE AERONAUTICAL LABORATORIES
CALIFORNIA INSTITUTE OF TECHNOLOGY

Unsplit Schemes for Hyperbolic Conservation Laws with Source Terms in One Space Dimension

M. V. Papalexandris, A. Leonard, and P. E. Dimotakis

GALCIT Report FM96-1

8 February 1996

Firestone Flight Sciences Laboratory

Guggenheim Aeronautical Laboratory

Karman Laboratory of Fluid Mechanics and Jet Propulsion

Pasadena

UNSPLIT SCHEMES FOR HYPERBOLIC CONSERVATION LAWS WITH SOURCE TERMS IN ONE SPACE DIMENSION

Miltiadis V. Papalexandris **, Anthony Leonard †, and Paul E. Dimotakis ‡

Graduate Aeronautical Laboratories
California Institute of Technology
Pasadena, CA 91125

Abstract.

The present work is concerned with the extension of the theory of characteristics to conservation laws with source terms in one space dimension, such as the Euler equations for reacting flows. New spacetime curves are introduced on which the equations decouple to the characteristic set of O.D.E's for the corresponding homogeneous laws, thus allowing the introduction of functions analogous to the Riemann Invariants. The geometry of these curves depends on the spatial gradients for the solution. This particular decomposition can be used in the design of efficient unsplit algorithms for the numerical integration of the equations. As a first step, these ideas are implemented for the case of a scalar conservation law with a non-linear source term. The resulting algorithm belongs to the class of MUSCL-type, shock-capturing schemes. Its accuracy and robustness are checked through a series of tests. The aspect of the stiffness of the source term is also studied. Then, the algorithm is generalized for a system of hyperbolic equations, namely the Euler equations for reacting flows. An extensive numerical study of unstable detonations is performed.

** Research Assistant, Aeronautics.

† Professor of Aeronautics.

‡ Professor of Aeronautics and Applied Physics.

Introduction.

Over the years, a large variety of efficient numerical schmes for hyperbolic systems of conservation laws has been developed. This progress came as a natural step following the understanding of fundamental concepts from the theory of nonlinear hyperbolic P.D.E's such as characteristic surfaces, existence, uniqueness, and solution of the Riemann problem, *etc.* See, for example, Courant and Hilbert (1963), Lax (1957), (1973), and Yee (1987) for an extensive review of the literature. Compressible, non-reacting flow was the main field of application of these schemes.

These high resolutions schemes, such as the ENO schemes, Harten *et al.* (1987), the MUSCL scheme, van Leer (1979), the PPM scheme, Colella and Woodward (1984), and Roe's approximate Riemann solver, Roe (1981), can be viewed as extensions to second-order accuracy of Godunov's original scheme. This is done by making use of the theory of characteristics for 2×2 systems of hyperbolic P.D.E's They employ locally, at each computational cell, the characteristic decomposition of the equations into a set of scalar fields in order to evaluate the flux terms at the cell interfaces. Discontinuous solutions can be computed by supplementing the characteristic equations with the appropriate jump relations, in other words by solving the corresponding Riemann problem.

Meanwhile, research in detonating flows had been pioneered by Von Neumann (1942), Zeldovich (1940), Doering (1943), and others 50 years ago. Numerical integration of the governing equations, in fine meshes, was initiated by Fickett and Wood (1966). Over the years considerable progress has been achieved in the study of the stability, see, *e.g.* Erpenbeck (1964), Lee and Stuart (1991), and the high- and low- frequency asymptotic nature of detonations, see, *e.g.* DiPerna and Majda (1985), Majda and Rosales (1984), (1987), Choi and Majda (1989), Majda and Roytburd (1992), Kapila *et al.* (1983), *etc.*

The highly-accurate algorithms for gas dynamics were first employed in detonation problems in the late '80s using splitting techniques, see *e.g.* Collela *et al.* (1986), Ben-Artzi (1989), and Yee (1987). Further development of these codes

and extensive numerical investigations were carried through to the 90's, see *e.g.* Bourlioux *et al.* (1991), Engquist & Sjogreen (1991), Lappas *et al.* (1993), Pember (1993), Quirk (1993), and LeVeque and Shyue (1995) *etc.* All these algorothms use a splitting technique, that is integration of the gas dynamic terms of the equations first, and integration of the appropriate O.D.E. for the source term in an intermediate step.

This decoupling can be done in an optimal way using Strang-type splitting, Strang (1968). Bounds for the $\mathcal{L}_1$ errors of splitting methods have been established for scalar conservation laws by Crandall and Majda (1980) for dimensional splitting in multi-dimensional homogeneous equations, and by Tang and Teng (1995) for time splitting in 1-D scalar laws with source terms. Nevertheless, this decoupling is artificial. The decomposition of the equations into scalar fields is not straightforward, *i.e.* the quantities dubbed as Riemann Invariants are now not constant along the characteristric trajectories. This error might be important in systems with multimode instabilities and multiplicity of spatial and temporal scales, such as the Euler equations for reacting flows.

Recently Lappas *et al.* (1994) developed an unsplit MUSCL-type scheme for the 2-D compressible Euler equations, based on the introduction of a family of space-time manifolds, dubbed as "Riemann Invariant Manifolds", along which the equations can be decomposed into the same scalar fields as in the 1-D case, and solved numerically. Their geometry depends on the spatial gradients of the flow. These manifolds provide, locally, a convenient system of coordinate system in space-time, and can be space-like or time-like depending on the flow gradients.

In the present paper the work of Lappas *et al.* (1994) is extended to systems of hyperbolic conservation laws with source terms, such as reacting, compressible flows. A new set of curves is defined, such that the O.D.E's that hold along these curves are the same as the O.D.E's that hold along the characteristics in the corresponding homogeneous case. The geometry of these curves depends locally on the spatial derivatives of the solution, and on the source terms. The introduction of this family of curves is believed to be very useful for the better understanding of the evolution

process described by the equations, and of the role that the source terms play in this process in particular.

The use of these curves also turns out to be very effective in the design of unsplit algorithms; an effort was made to remove the error induced by splitting, by constructing algorithms in which the integration of the equations, including the contributions of the source terms, is performed in a single, fully-coupled step. This is achieved by tracing the afore-mentioned curves in space time, in a way completely analogous to the tracing of the characteristic curves in the homogeneous case.

The first part of this paper deals with the development of these ideas in the case of a scalar law with a nonlinear source term. Extensive numerical experimentation has been performed. The results are compared with approximate solutions or exact solutions whenever possible. The role of the stiffness of the source term, has been also examined. The second part deals with the unsteady, Euler equations for reacting flows in one space dimension. Comparisons with results obtained by conventional schemes are made.

1. Study of the inviscid Burgers equation with a nonlinear source term.

1.1 General Formulation.

Consider the following Initial Value Problem for the scalar $u(x,t)$:

$$\frac{\partial}{\partial t}u + \frac{\partial}{\partial x}f(u) = g(u), \quad x \in [0,\infty) \tag{1.1a}$$

$$u(x,0) = u_0(x) \in [0,1], \tag{1.1b}$$

The corresponding homogeneous law is associated with a convex entropy pair, *i.e.* *the entropy function:* $\phi(u)$, and *the entropy flux:* $\psi(u)$, satisfying

$$\psi_u = \phi_u f_u .$$

The entropy pair is subject to the following *entropy condition*:

$$\frac{\partial}{\partial t}\phi(u) + \frac{\partial}{\partial x}\psi(u) \leq 0 \tag{1.2}$$

Furthermore, the source term $g(u)$ is assumed to satisfy

$$g(u) \in \mathcal{C}^2([0,1], \Re) \tag{1.3a}$$

$$g(0) = 0 = g(1). \tag{1.3b}$$

Let $\Omega = [0,\infty) \times [0,T]$. A bounded measurable function, u, is a weak solution of (1.1) if $\forall \xi \in \mathcal{C}^1(\Omega)$ with compact support in $([0,\infty) \times [0,T))$

$$\int\int_{\Omega} (u\xi_t + f(u)\xi_x) dx\, dt + \int_0^{\infty} u_0(x)\xi(x,0)\, dx = -\int\int_{\Omega} \xi\, g\, dx\, dt \tag{1.4}$$

Existence and uniqueness of weak solutions for the above problem was given by Kruzkov (1970). The source term $g(u)$, which is constructed to possess two equilibrium values at $u = 0$ and $u = 1$, can be either *dissipative* or *non-dissipative*. A source term is defined to be dissipative if, following Chen *et al.* (1994),

$$\frac{\partial \phi(u)}{\partial u} g(u) \leq 0, \quad \text{for all } u \tag{1.5}$$

where $\phi(u)$ is the convex entropy function associated with the corresponding homogeneous law. The distinction between dissipative and non-dissipative source term is made because the large-time solution of the above IVP may approach one equilibrium value or another,depending on the nature of the source term. It might be obvious to the reader, but it should be stated, that the decay estimates for the corresponding homogeneous law, Lax (1957), (1973), do not hold for the above problem.

The characteristic decomposition of the problem yields:

$$\frac{\mathrm{d}u}{\mathrm{d}t} = g(u), \quad \text{along} \quad \frac{\mathrm{d}x}{\mathrm{d}t} = f_u$$

Motivated by the fact that for the corresponding homogeneous law, u remains constant along characteristics, someone could ask the question: *Along which curve in space time does u remain constant?* The answer is that at smooth parts of the flow

$$\frac{\mathrm{d}u}{\mathrm{d}t} = 0, \quad \text{along} \quad \frac{\mathrm{d}x}{\mathrm{d}t} = f_u - \frac{g(u)}{\partial u/\partial x}. \tag{1.6}$$

The geometry of this curve depends locally on the spatial derivatives of the solution. This however should not be disturbing because the derivatives are known for any time the solution itself is known, *i.e.* we have all the necessary elements to construct this curve in space-time, without extra cost.

1.2 Description of the Algorithm and Numerical Results.

Consider the Initial Value Problem formulated as above, when $f(u) = u^2/2$:

$$\frac{\partial}{\partial t}u + \frac{\partial}{\partial x}\left(\frac{u^2}{2}\right) = g(u), \quad x \in [0,\infty) \tag{1.7a}$$

$$u(x,0) = u_0(x) \in [0,1]. \tag{1.7b}$$

A typical nonlinear non-dissipative term satisfying $(1.3a)$, $(1.3b)$ is

$$g(u) = \frac{1}{\varepsilon}u(1-u) \tag{1.8}$$

where ε is a coefficient measuring the stiffness of the system. An entropy pair associated with the corresponding homogeneous law is given by:

$$\phi(u) = u^2 \quad \psi(u) = \frac{2}{3}u^3\,. \tag{1.9}$$

In the case where the source term is given by (1.8), and for smooth $u_0(x)$ the equation of the characteristic decomposition yields:

$$u(x,t) = u_0\,\frac{e^{t/\varepsilon}}{1+(e^{t/\varepsilon}-1)u_0}, \tag{1.10a}$$

along the curves

$$x = x_0 + \varepsilon \log\left[1+(e^{t/\varepsilon}-1)u_0\right] \tag{1.10b}$$

Given the above relation, one can deduce the following shock-formation criterion: *For the I.V.P. given by relations* (1.7), *and* (1.8), *a shock will form if the following inequality is satisfied:*

$$u_0(x) + \varepsilon u_0'(x) < 0 \quad \text{for some } x. \tag{1.11}$$

where $u_0'(x)$ is the derivative of $u_0(x_0)$. The shock-formation time is given by:

$$t_{s.f.} = \varepsilon \log\left(\frac{A(x)-1}{A(x)}\right), \quad A(x) \equiv (u_0(x) + \varepsilon u_0'(x))_{\min}. \tag{1.12}$$

The equation of the curves in space-time along which u remains constant is given by

$$\frac{\mathrm{d}x}{\mathrm{d}t} = u - \frac{g(u)}{\partial u/\partial x} \equiv v(x,t) \tag{1.13}$$

The issue of the limit case $\partial u/\partial x \to 0$ will now be addressed. First it should be noticed that at the points in the $x-t$ plane where the spatial derivative of the solution approaches zero, there is no singularity of the equation. The curve defined by (1.13) becomes locally parallel to the $x-$axis at those points. Obviously then, it can not be used for computational purposes, in the evaluation of the fluxes at the interfaces. However, the knowledge that the derivative of the solution vanishes at those points can be used instead, such that the desired degree of accuracy be maintained. In the following it will be shown how these ideas can be combined in a simple and uniform manner.

It is worth pointing out, in order to pursuade the somewhat more sceptical reader, that a similar phenomenon can occur in the application of shock-capturing schemes for the numerical solution of Hamilton-Jacobi type equations. A well known example is the computation of moving fronts whose speed is curvature-dependent, Osher & Sethian (1988), Sethian (1990). The equivalent situation there arises when the speed of the front is locally zero. No serious difficulties have been reported by the authors in the computations at these points.

The algorithm proposed for the numerical integration of the above problem belongs to the class of 2^{nd} order accurate MUSCL-type schemes, and is described below.

Consider uniform spacing in the $x-$direction of length Δx and let u_j^n be the approximate average of u in the j^{th}-cell at time $t = n\,\Delta t$.

$$u_j^n \approx \frac{1}{\Delta x}\int_{(j-1/2)\Delta x}^{(j+1/2)\Delta x} u(x,\, n\,\Delta t)\,\mathrm{d}x \tag{1.14a}$$

Assume linear interpolation of $u(x,\, n\Delta t)$ at each cell:

$$u(x,\, n\Delta t) \;=\; u_j^n \,+\, (u_x)_j\, x\,, \quad x \,\epsilon\, \left[-\frac{\Delta x}{2}\,,\, \frac{\Delta x}{2}\right] \tag{1.14b}$$

The slope of $u(x,t)$ on each cell, $(u_x)_j$, can be computed using a standard TVD limiter. In the present algorithm van Leer's limiter was chosen, van Leer (1984):

$$(u_x)_j \;=\; \text{ave}(u_x^-\,,\, u_x^+), \tag{1.15a}$$

where,

$$u_x^- \;=\; \frac{u_j^n - u_{j-1}^n}{\Delta x}\;, \qquad u_x^+ \;=\; \frac{u_{j+1}^n - u_j^n}{\Delta x}, \tag{1.15b}$$

$$\text{ave}(a,b) \;\equiv\; \frac{a+b}{2}\left(1 \,-\, \frac{(a-b)^2}{a^2+b^2+c^2}\right) \tag{1.15c}$$

and c is a small number, $(c^2 \,\ll\, 1)$.

The conservation law (1.7) is approximated by the following explicit finite difference scheme:

$$u_j^{n+1} \;=\; u_j^n - \frac{\Delta t}{\Delta x}\left(\frac{(u_{j+1/2}^{n+1/2})^2}{2} - \frac{(u_{j-1/2}^{n+1/2})^2}{2}\right) + \frac{\Delta t}{2}\left(g\left(u_{j+1/2}^{n+1/2}\right) + g\left(u_{j-1/2}^{n+1/2}\right)\right) \tag{1.16}$$

In the above relation $u_{j+1/2}^{n+1/2}$ denotes the value of u at the right interface of the j^{th}-cell at a time $t = (n+1/2)\,\Delta t$. It is evaluated by tracing forward in time the constant-u curve, as given by (1.13). This is done by approximating that curve locally by a straight line and locating the point x_p that satisfies $u(x_p, n\Delta t) = u_{j+1/2}^{n+1/2}$.

The above relation, which is really a discretization of the equation $\mathrm{d}u = 0$ that holds along the "invariant" curve (1.13), must be supplemented by the appropriate jump relations that take care of discontinuities, i.e an appropriate Riemann problem has to be solved locally at the interface. The Riemann problem for the corresponding homogeneous law (*i.e.* inviscid Burgers equation) admits a self-similar solution, depending on x/t only, see for example Lax (1973). For the non-homogeneous conservation law, the Rankine-Hugoniot relation remains the same, but the rarefaction

wave no longer admits a self-similar representation. However, as $x \to 0$, $t \to 0$, the solution of the non-homogeneous case approaches the self-similar solution of the corresponding homogeneous problem. Therefore, for computational purposes, we can use the self-similar solution without loss of accuracy. For the conservation law under consideration, and given the fact that $u(x,t) > 0$ (thus only shocks that propagate to the right are acceptable), the numerical solution of the Riemann problem reduces to the following procedure:

Let u_L, u_R the solution at the left and right side of the j^{th} interface:

$$u_L = u_j^n + \frac{\Delta x}{2}(u_x)_j$$

$$u_R = u_{j+1}^n - \frac{\Delta x}{2}(u_x)_{j+1},$$

and let $\Delta u = u_R - u_L$. Let $u(x_p, n\Delta t)$ be the value evaluated by tracing the invariant curve (1.13) in time, as described above, and let $v(x_p, n\Delta t)$ be the tangent of (1.13) passing through $(x_p, n\Delta t)$. Then, $u_{j+1/2}^{n+1/2}$ is given by:

$$u_{j+1/2}^{n+1/2} = \begin{cases} u(x_p, n\Delta t), & \text{if } v(x_p, n\Delta t) > 0 \\ u(x_p, n\Delta t) - \Delta u, & \text{if } v(x_p, n\Delta t) < 0 \end{cases}$$

As already mentioned above, in the absence of discontinuities the above procedure gives:

$$u_{j+1/2}^{n+1/2} = u(x_p, n\Delta t) = u_j^n + \frac{\Delta t}{2} \frac{\left(\frac{\Delta x}{\Delta t} - u_j^n\right)(u_x)_j - g\left(u_j^n\right)}{1 + \frac{\Delta t}{2}(u_x)_j - \frac{\Delta t}{2}\frac{\partial}{\partial x} g\left(u_j^n\right)} \tag{1.17}$$

At the limit $u_x \to 0$ the above relation reduces to an explicit, 2^{nd} order accurate scheme based on Taylor series expansion:

$$u_{j+1/2}^{n+1/2} = u_j^n + \frac{\Delta x}{2}(u_x)_j + \frac{\Delta t}{2}(u_t)_j$$

Note, however, that if a CFL condition were to apply, then

$$\frac{\Delta t}{\Delta x} |v|_{\max} \leq 1, \tag{1.18}$$

Consequently very small values of the spatial derivatives of the solution might lead to small time step. Therefore for the cells where the slope is zero and their neighboring cells, it would be better to find the solution at the interfaces at $t = (n + 1/2)\Delta t$ by taking the Taylor expansion around u_j^n. For this particular scalar example, the Taylor expansion and (1.17) are identical, hence no modification is necessary.

Finally, it should be pointed out that any interpolation procedure can be implemented with the algorithm, because the interpolation step is in principle independent of the effort to create unsplit schemes. This step, however, plays a very important role in the accuracy of any shock-capturing method. This is more so in the present case, because efficiency and robustness of the scheme depend greatly on the accuracy with which the "invariant" curve (1.13) is known, and hence on the accuracy with which the spatial derivatives of the solution are approximated.

As a first test of the scheme, the source term given by (1.8) was considered, with ε set equal to 1. Initial and Boundary Conditions were given by:

$$u_0(x_0) = \begin{cases} x_0\,(1 - x_0)\,, & \text{if } x \leq 1 \\ 0\,, & \text{if } x > 1 \end{cases} \tag{1.19}$$

and,

$$u(0,t) = 0\,,\ u(\infty,t) = 0\,, \quad \forall\, t \tag{1.20}$$

The results obtained for this problem are given in Fig. 1. For this test case, $CFL = 0.6$. A shock will form at time $t = 0.61803$. The value of u behind the shock will increase because of the source term until u becomes equal to 1, which is the upper equilibrium value. From then on, the shock will propagate with a speed $s = 0.5$. The whole evolution process was captured quite well by the present scheme.

As a second test, the Initial Conditions of the previous problem were changed to:

$$u_0(x_0) = \begin{cases} 1\,, & \text{if } \Delta x < x \leq 1 \\ 0\,, & \text{if } x > 1, \text{or } 0 < x < \Delta x \end{cases} \tag{1.21}$$

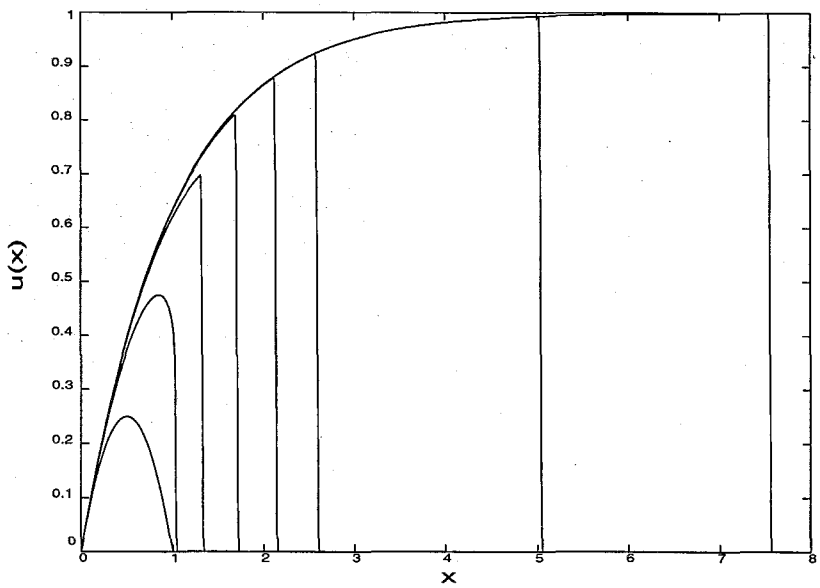

FIG. 1 Spatial profiles for the case where $g(u) = u(1-u)$, and I.C's, and B.C's given by (1.19) and (1.20) respectively. Profiles at $t = 0.0,\ 1.0,\ 2.0,\ 3.0,\ 4.0,\ 5.0,\ 10.0,\ 15.0$. $\Delta x = 0.02$.

The results obtained for this problem are given in Fig. 2. For this test case, $CFL = 0.6$. The left discontinuity, initially at $x = 1$, will become a rarefaction wave. The head of this expansion, which is an "acoustic" disturbance, will move with characteristic speed $u_{ch} = 1.0$, while the tail will stay at the origin because the characteristic speed there is zero. The right discontinuity will move with shock speed $s = 0.5$. As soon as the head of the expansion reaches the shock, the shock should start to decay. This decay, however will stop because of the source term which will eventually restore the post-shock value at the upper equilibrium level.

Consider now the following Riemann problem,

$$u_0(x_0) = \begin{cases} 0, & \text{if } 0 \leq x \\ 1, & \text{if } x > 0 \end{cases} \tag{1.22}$$

For this particular problem we can use (1.10a) and (1.10b) to get the expression of the resulting rarefaction in closed form:

$$u(x,t) = \begin{cases} \frac{e^{t/\epsilon}\left(e^{x/\epsilon}-1\right)}{e^{x/\epsilon}\left(e^{t/\epsilon}-1\right)}, & \text{if } x \leq t \\ 1, & \text{if } x > t \end{cases} \tag{1.23}$$

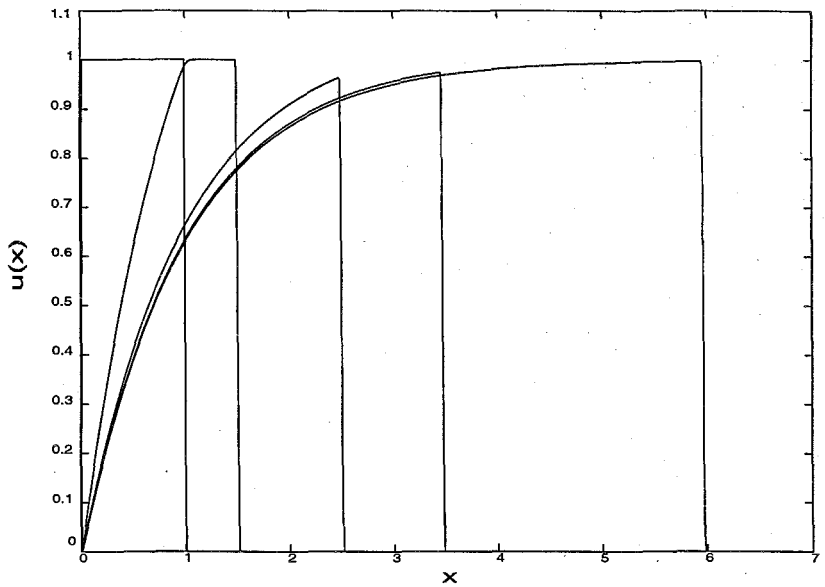

FIG. 2 Spatial profiles for the case where $g(u) = u(1-u)$, and B.C's, and I.C's given by (1.20) and (1.21) respectively. Profiles at $t = 0.0, 1.0, 3.0, 5.0, 10.0$. $\Delta x = 0.02$.

The computed rarefaction, as shown in Fig. 2, (and for the times that the post-shock value is 1.0, so that u gets the equilibrium values at the endpoints of the rarefaction), are in excellent agreement with the above relation.

To demonstrate the difference between a dissipative and a non-dissipative source term, the same probem as before was considered but now the source term was given by

$$g(u) \;=\; -\frac{1}{\varepsilon}u\,(1-u) \tag{1.24}$$

The above relation differs from (1.8) only in the sign of the source term. Expressions for the characteristics and shock-formation criterion can be derived for this case, too. Numerical results for this problem are shown in Fig. 3. Again, they were obtained with $CFL = 0.6$. Note that the shock wave decays with a rate faster than $O(1/\sqrt{t})$, which is the decay rate for a shock wave in the corresponding homogeneous law. It is also interesting to notice that the rarefaction waves are convex functions, in contrast with the case of a dissipative source term where the rarefactions are concave.

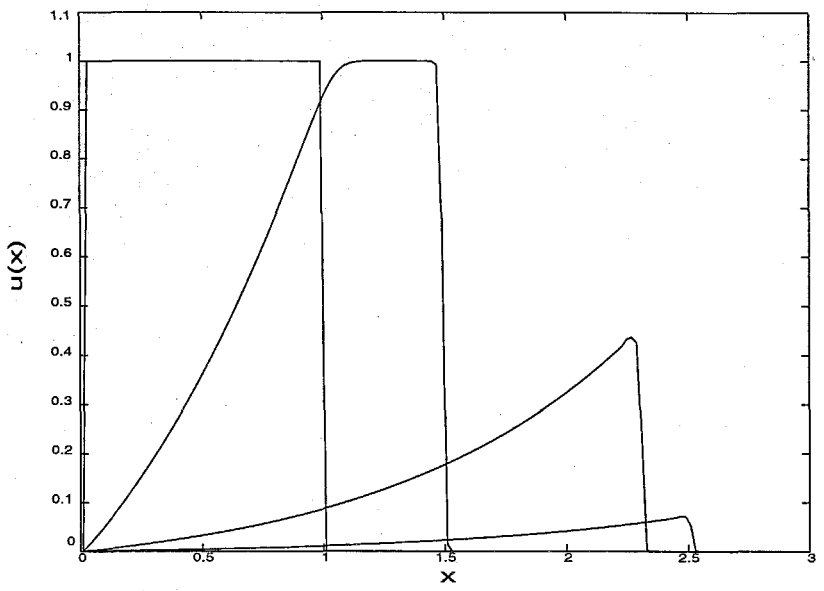

FIG. 3 Spatial profiles for the case where $g(u) = -u(1-u)$, and B.C's, and I.C's given by (1.20) and (1.21) respectively. Profiles at $t = 0.0, 1.0, 3.0, 5.0$. $\Delta x = 0.02$.

The issue of the stiffness of the source term will now be discussed. Many authors have devoted attention to the numerical integration of hyperbolic P.D.E's with stiff source terms and the spurious solutions that might be obtained, see for example Colella *et al.* (1986), LeVeque and Yee (1990), Bourlioux (1991), and Griffiths *et al.* (1992). Despite the fact that shock capturing schemes are stable even in the stiff cases, coarse spatial resolution will give incorrect propagation speeds of discontinuities. This is because the source terms are activated in all the region occupied by the smeared shock, in a non-physical manner. The result is a spurious shock speed, usually of one cell per time-step for coarse resolutions.

It is also acknowledged, Bourlioux (1991), that finer temporal resolutions will produce shock speeds of one cell per $2-3$ timesteps. Pember, (1992), also points that out, and he finds spurious speeds in travelling-wave solutions. Additionally he conjectures a criterion for the non-appearance of spurious solutions in implicit split schemes for dissipative 2×2 systems, namely the commutability of the vanishing viscosity limit for viscous regularization of (1.7), and the limit of infinite stiffness.

Liu (1987) and Chen *et al.* (1992) show that for dissipative 2×2 systems this commutability holds.

In the present numerical investigations the focus is on the non-dissipative scalar law given by (1.7), (1.8). The proposed scheme is compared with its equivalent split scheme, that is

$$u^{n+1} = \mathcal{L}_{\mathcal{S}}{}^{(\Delta t/2)}\, \mathcal{L}_{\mathcal{F}}{}^{(\Delta t/2)}\, \mathcal{L}_{\mathcal{S}}{}^{(\Delta t/2)}\, u^n \tag{1.25}$$

Here, $\mathcal{L}_{\mathcal{F}}$ is the numerical solution operator for the corresponding homogeneous conservation law

$$\frac{\partial u}{\partial t} + \frac{\partial}{\partial x}\left(\frac{u^2}{2}\right) = 0. \tag{1.26}$$

It is a MUSCL-type algorithm like the nonlinear version of scheme III by van Leer (1977). The flux at the interfaces at time $t = (n+1/2)\Delta t$ are evaluated by tracing the characteristic $\mathrm{d}x/\mathrm{d}t = u$ and solving the Riemann problem associated with (1.26). $\mathcal{L}_{\mathcal{S}}$ is the numerical solution operator for the O.D.E.

$$\frac{\mathrm{d}u}{\mathrm{d}t} = g.$$

i.e.

$$\mathcal{L}_{\mathcal{S}}{}^{(\Delta t/2)}(u) = u + \frac{\Delta t}{2} g(u)$$

It could argued that a more efficient split scheme could have been considered, such as an implicit one. But then again, the same is true for the unsplit scheme; the implicit version of this scheme for a scalar law can be easily implemented. The choice was made among 2^{nd} order accurate schemes that have already been used in systems of P.D.E's such as the Euler equations. The MUSCL algorithm used in the split scheme is generally regarded as one of the most efficient schemes in the literature.

As a first test, the following conditions were given

$$u_0(x_0) = \begin{cases} 1, & \text{if } x \leq 1 \\ 0, & \text{if } x > 1 \end{cases} \tag{1.27a}$$

with

$$u(0,t) \;=\; 1\,, \quad u(\infty,t) \;=\; 0, \quad \forall t, \tag{1.27b}$$

For both algorithms the discretization was

$$\Delta x \;=\; 0.02\,, \quad \Delta t \;=\; 0.01\,.$$

Results for $\varepsilon = 0.01,\ 0.02,\ 0.03,\ 0.05,\ 0.07$ are given at the Figs. 4. The relative error:

$$\frac{(u_{\text{computed}} \;-\; u_{\text{exact}})}{u_{\text{exact}}}\,, \tag{1.28}$$

based on the level set $u(x,t) = 0.5$, is drawn for both schemes in Fig. 5. Both schemes give wrong speeds if $\Delta t/\varepsilon \;> O(1/3)$. By the term *wrong speed* an error of 20% or more is assumed. The unsplit scheme, however, seems to work a little better than the split scheme in the cases were the above ratio is kept small. For $\varepsilon > 0.1$ both schemes had en error less than 10%. For values of ε less than 0.01 the computed wave speeds were one cell per time step. The numerical solutions went unstable when $\varepsilon = O(10^5)$ with both schemes.

Next the issue of wrong travelling-wave solutions is examined. As before, the conservation law (1.7) with a source term given by (1.8) . Initial and Boundary conditions are given by

$$u_0(x) \;=\; e^{-x} \tag{1.29a}$$

$$u(0,t) \;=\; 1\,, \quad u(x \to \infty, t) \;=\; 0\,, \quad \forall\, t \tag{1.29b}$$

For the above problem a shock will never form, according to (1.11). Combining equations (1.10a) and (1.10b) , we deduce the following expression for $u(x,t)$:

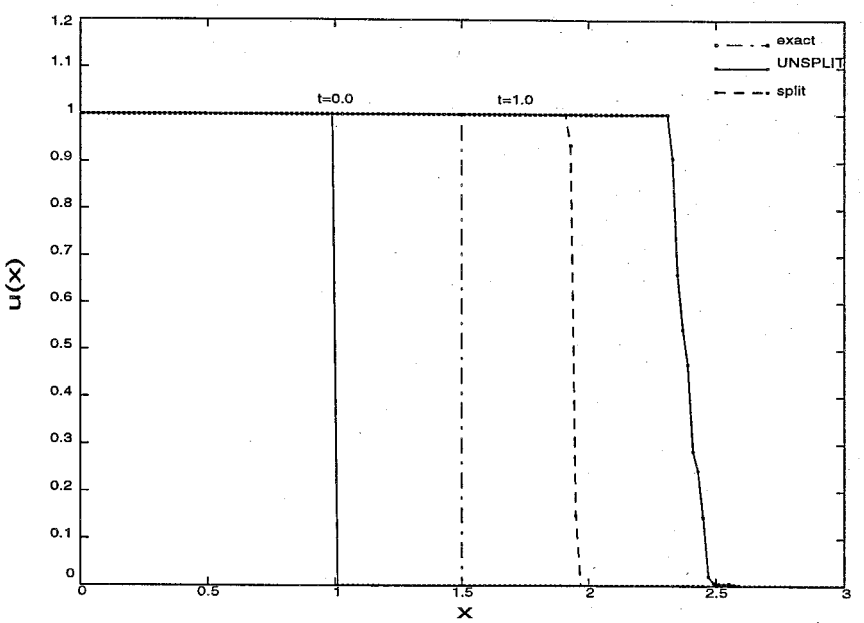

FIG. 4a Performance of unsplit *vs.* split algorithm for the problem given by (1.7), (1.8), (1.27) for $\varepsilon = 0.01$.

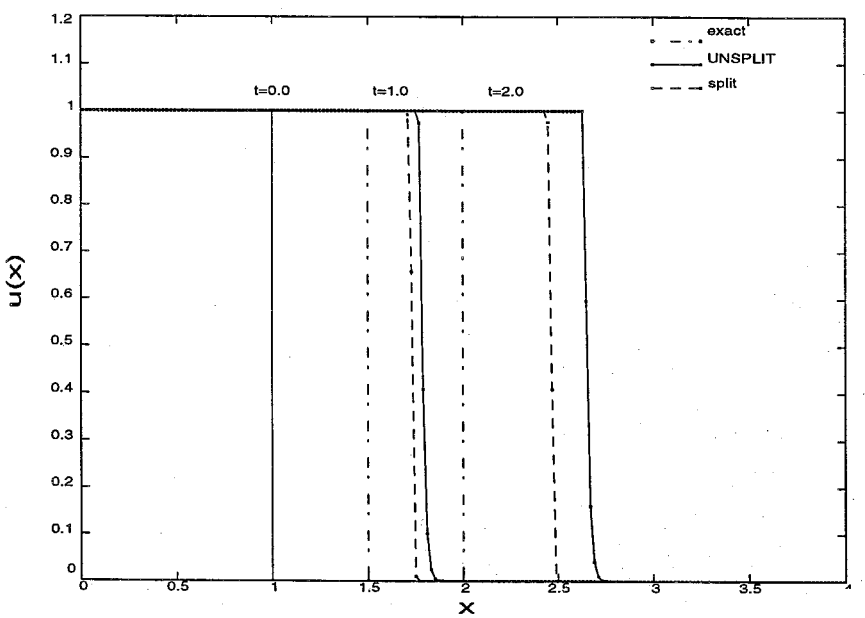

FIG. 4b Performance of unsplit *vs.* split algorithm for the problem given by (1.7), (1.8), (1.27) for $\varepsilon = 0.02$.

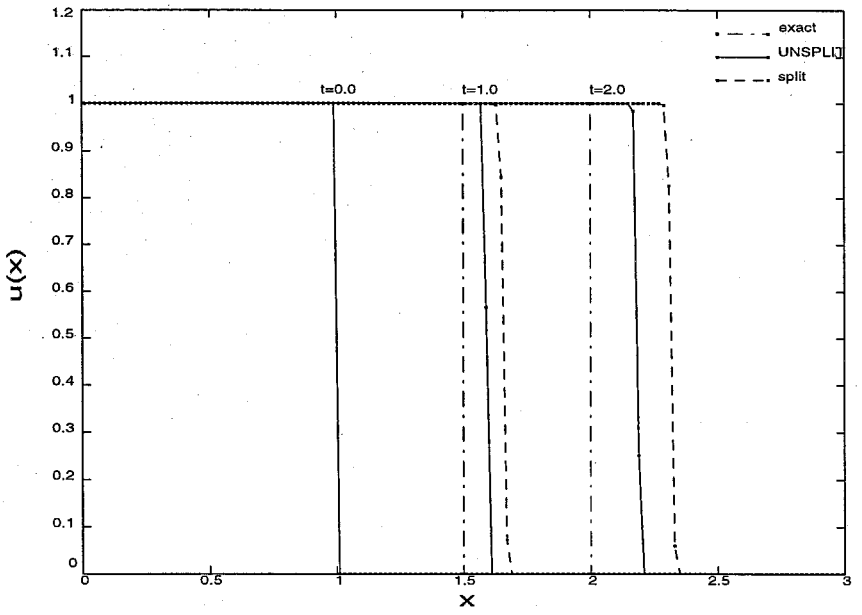

FIG. 4c Performance of unsplit *vs.* split algorithm for the problem given by (1.7), (1.8), (1.27) for $\varepsilon = 0.03$.

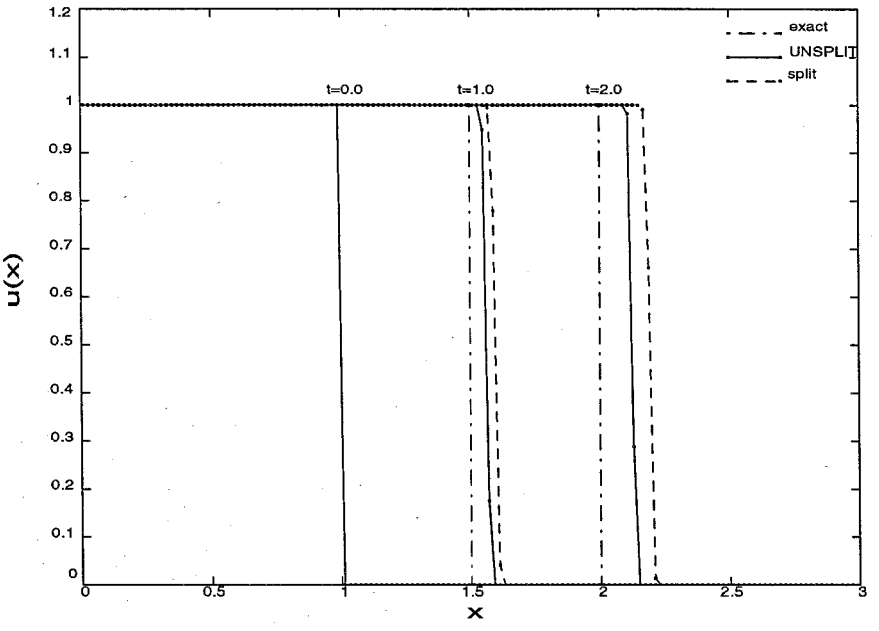

FIG. 4d Performance of unsplit *vs.* split algorithm for the problem given by (1.7), (1.8), (1.27) for $\varepsilon = 0.05$.

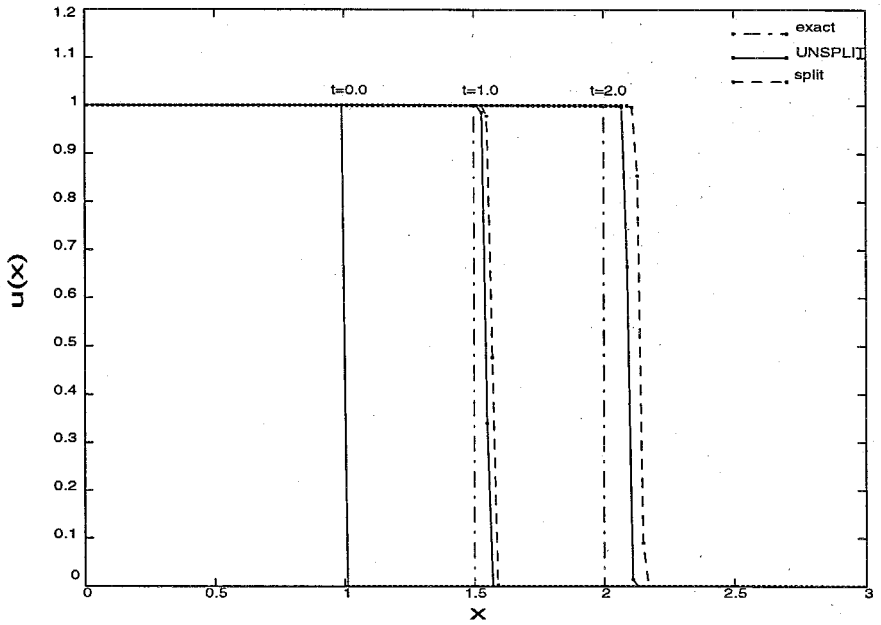

FIG. 4e Performance of unsplit *vs.* split algorithm for the problem given by (1.7), (1.8), (1.27) for $\varepsilon = 0.07$.

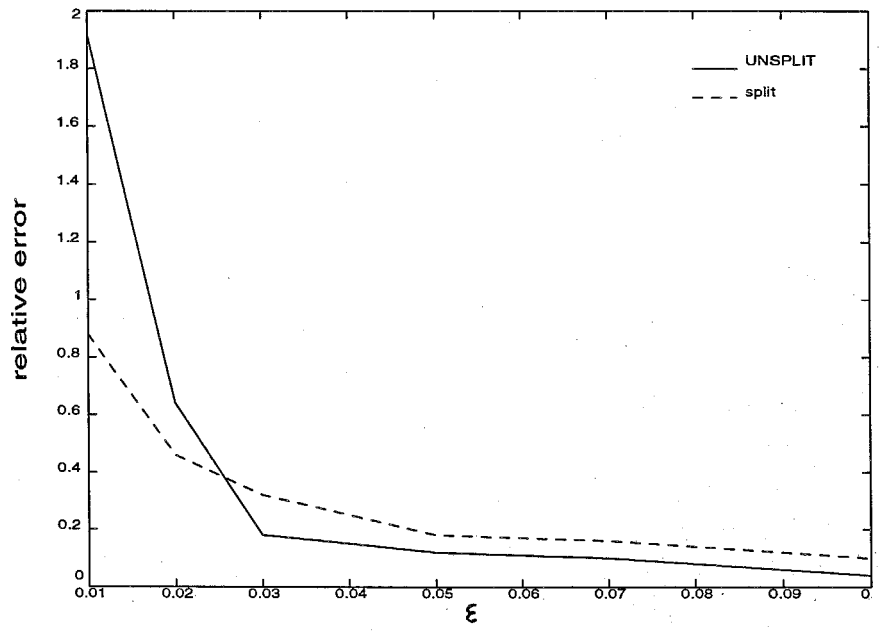

FIG. 5 Relative error as defined by (1.28) *vs.* ε for the split and unsplit algorithm.

$$u(x,t) = \begin{cases} 1, & \text{if } x \leq t \\ e^{t-x}\left[u(x,t) + e^{t/\varepsilon}\left(1 - u(x,t)\right)\right]^{1-\varepsilon}, & \text{if } x > t \end{cases}$$

Then, for $\varepsilon \ll 1$, the following approximation holds (hereafter called as the *analytical expression*):

$$u(x,t) = \begin{cases} 1, & \text{if } x \leq t \\ \frac{e^{-(x-t)}}{e^{-t/\varepsilon} + e^{-(x-t)}\left(1 - e^{-t/\varepsilon}\right)}, & \text{if } x > t \end{cases} \tag{1.30}$$

Essentially, this is a wave travelling with speed

$$c_{\text{t.w.}} = \frac{1}{\varepsilon} + 1$$

The acoustic disturbance, located at $x = t$, and initially set at the origin, travels with speed equal to 1. Results for this case obtained by the split and the unsplit scheme are presented in Fig. 6, for $\varepsilon = 0.01$. The analytical solution given by (1.20) was drawn, for comparison purposes. The unsplit scheme performed much better than the corresponding split one. In both cases (split and unsplit) presented, the ratio $\Delta t/\Delta x$ was taken at $\Delta t/\Delta x = 0.5$ (note that in this test case the maximum characteristic speed is 1, therefore this ratio corresponds to the value of the "classical" CFL number). When that ratio was lowered to a value of 0.25, the unsplit scheme was again superior; see Fig. 6c.

For $\varepsilon = 0.01$ the relative error

$$\left| \frac{\left(c_{\text{computed}} - c_{\text{t.w.}}\right)}{c_{\text{t.w.}}} \right|$$

in the calculation of the speed of the travelling wave against the inverse of the resolution $1/\Delta x$, is presented in Fig. 7, for both schemes.The calculation of the speed was based on the level set $u(x,t) = 0.5$. It can be seen for example, that with resolution $\Delta x = 0.02$, the relative error with the split scheme is four times higher than the relative error with the unsplit scheme. Similar performance was observed for higher values of ε.

In Fig. 8, parametric curves of that error are plotted as a function of the stiffness coefficient and the resolution, for both schemes. It is seen, for example, that in order to obtain results within a 10% error, the resolution at the unsplit scheme has to be almost three times smaller than the resolution required by the unsplit scheme. For higher accuracy the ratio of the acceptable resolutions is even higher.

To demonstrate the overall effectiveness, (*i.e.* even for non-stiff problems) of the unsplit scheme over traditional methods, the previous test case was run again, but now the stiffness coefficient ε was taken equal to unity. For that particular problem the exact solution is given by:

$$u(x,t) = \begin{cases} 1, & \text{if } x \leq t \\ e^{t-x}, & \text{if } x > t \end{cases}$$

i.e. it is a travelling wave with speed 1. The resolution used for this problem was $\Delta x = 0.5$. For finer resolutions the difference in the results obtained by the two methods was minimal. The ratio $\Delta t/\Delta x = 0.5$ was used. The results are shown in Fig. 9. Obviously the unsplit scheme still performs better, but the improvement over the results taken by the split scheme is not as much as in the cases with stiff source terms.

To summarize the numerical investigation for the accuracy of the proposed scheme, it was observed that neither the proposed scheme nor the split one give accurate wave speeds if the time-step is not considerably smaller than the stiffness coefficient, ε. This is not surprising because both schemes are explicit, therefore resolution of the smallest time scale is necessary. However for reasonable time-steps, the unsplit scheme is considerably more accurate, particularly in cases characterized by a large value of the stiffness coefficient.

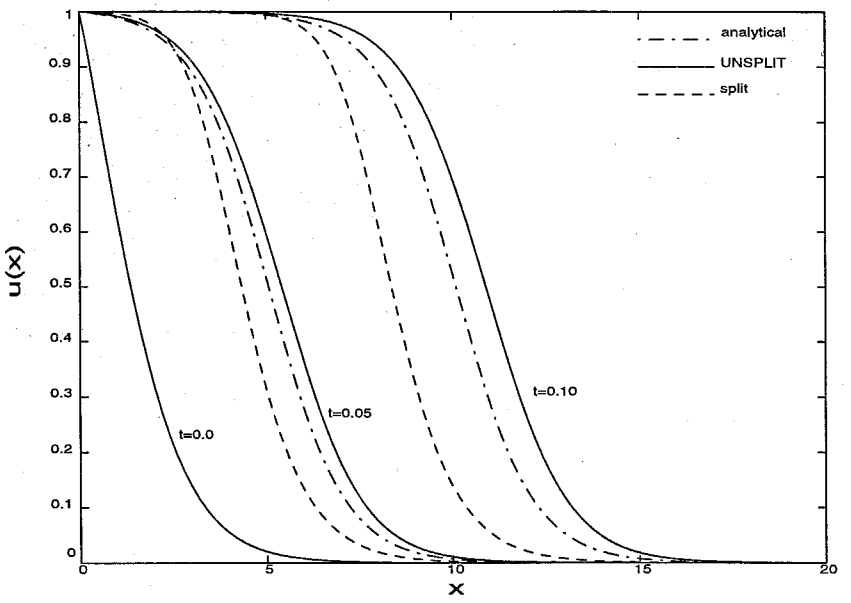

FIG. 6a Performance of unsplit *vs.* split algorithm for the problem given by (1.7), (1.8), (1.29) for $\varepsilon = 0.01$. Discretization: $\Delta x = 0.02$, $\Delta t = 0.01$.

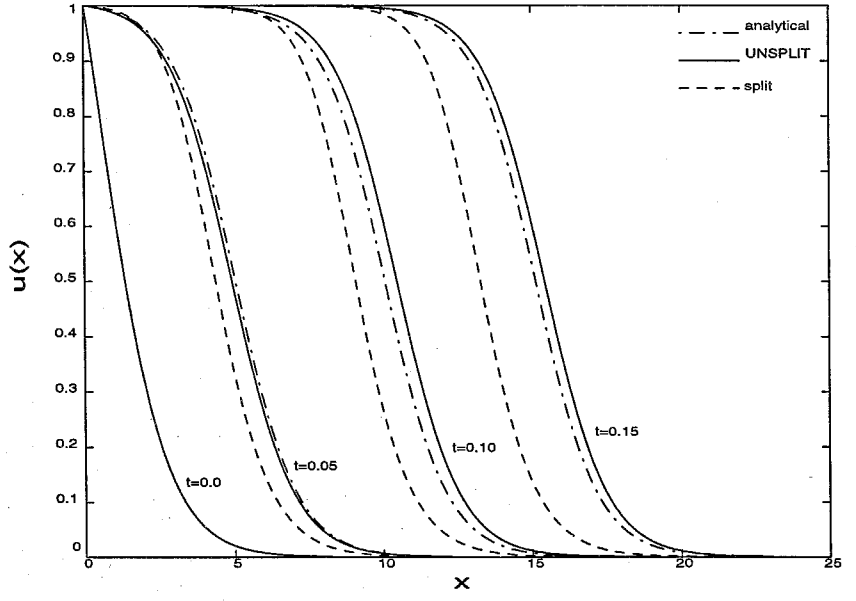

FIG. 6b Performance of unsplit *vs.* split algorithm for the problem given by (1.7), (1.8), (1.29) for $\varepsilon = 0.01$. Discretization: $\Delta x = 0.01$, $\Delta t = 0.005$.

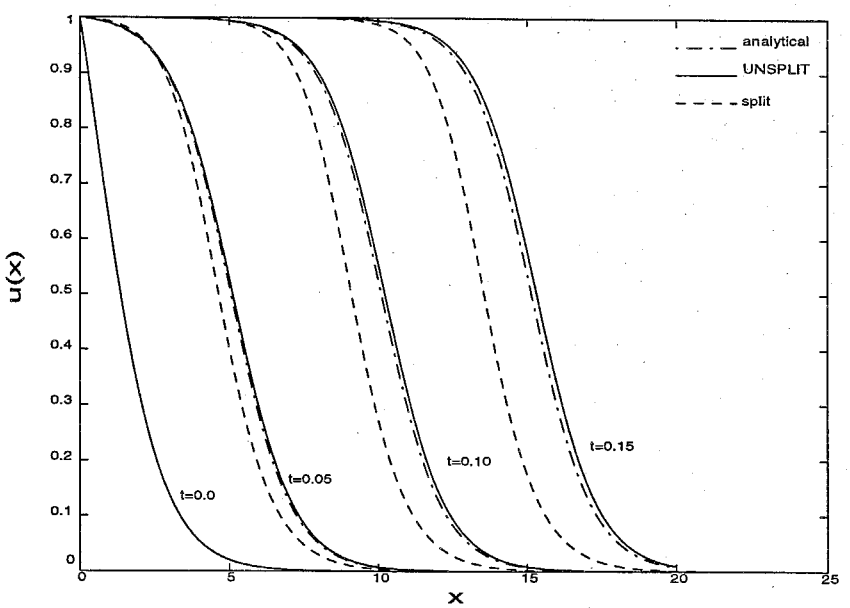

FIG. 6c Performance of unsplit *vs.* split algorithm for the problem given by (1.7), (1.8), (1.29) for $\varepsilon = 0.01$. Discretization: $\Delta x = 0.02$, $\Delta t = 0.005$.

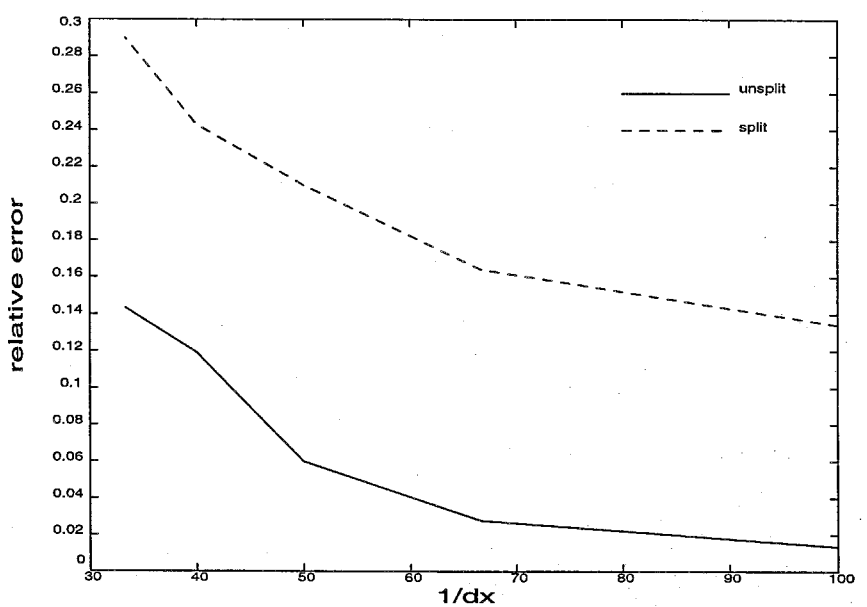

FIG. 7 Relative error in the calculation of the speed of the travelling wave for the problem given by (1.7), (1.8), (1.29) for $\varepsilon = 0.01$. All computations were performed with $\Delta t/\Delta x = 0.5$.

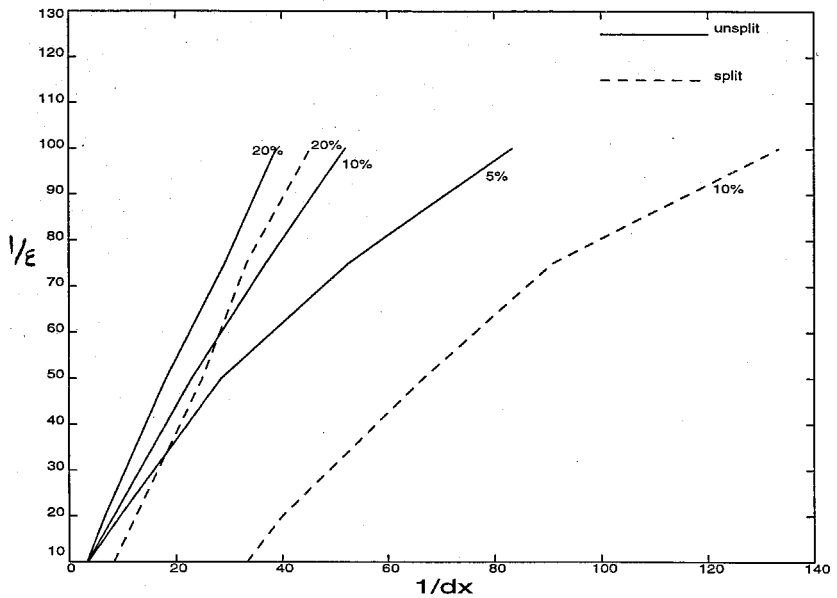

FIG. 8 Error curves in the calculation of the speed of the travelling wave for the problem given by (1.7), (1.8), (1.29) for various ε. All computations were performed with $\Delta t/\Delta x = 0.5$.

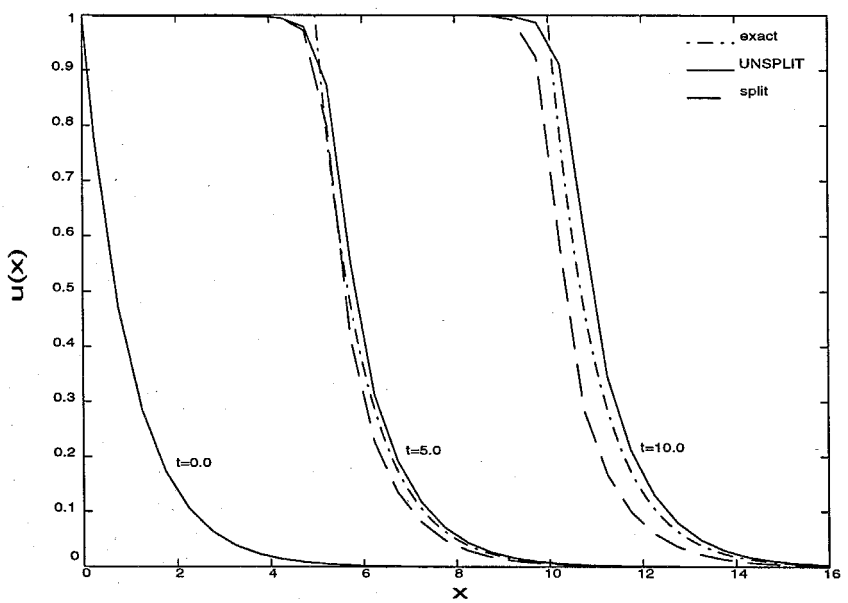

FIG. 9 Performance of unsplit *vs.* split algorithm for the problem given by (1.7), (1.8), (1.29) for $\varepsilon = 1.0$. Discretization: $\Delta x = 0.5$, $\Delta t = 0.25$

2. Study of the Euler equations for chemically reacting flows.

The decomposition performed previously for the scalar conservation law is extended to systems of equations in one space dimension. An unsplit numerical scheme has been designed based on this decomposition. This algorithm is used in the numerical study of unstable one-dimensional detonations. The case of detonation problems is particularly interesting as regards applications; but it is also very difficult to simulate numerically. This difficulty is mainly due to the large number of time-scales and length-scales associated with these problems.

2.1 General Formulation.

A homogeneous first order system of n quasilinear equations in two independent variables (x,t)

$$\frac{\partial U}{\partial t} + \frac{\partial F(U)}{\partial x} = 0\,, \tag{2.1}$$

where $U = (u_1, ..., u_n)$ is the solution vector, and $F(U)$ is the corresponding flux vector, is called hyperbolic if the Jacobian $DF(U)$ possesses real eigenvalues λ_j, $j = 1, ..., n$. As usual, one could write the above system in *characteristic* form:

$$\mathbf{l}_j \cdot \left(\frac{\mathrm{d}U}{\mathrm{d}t}\right)_j = 0, \quad j = 1, ..., n. \tag{2.2}$$

with

$$\left(\frac{\mathrm{d}}{\mathrm{d}t}\right)_j \equiv \frac{\partial}{\partial t} + \lambda_j \frac{\partial}{\partial x}\,, \tag{2.3}$$

(repeated index does not imply summation). This is done by performing the following two algebraic steps:

1. Evaluate the eigenvalues of the Jacobian $DF(U)$, and the corresponding left and right eigenvectors, $\mathbf{l}_j = (l_1, ..., l_n)_j$ and $\mathbf{r}_j = (l_1, ..., l_n)_j$ respectively, $j = 1, ..., n$,
2. Multiply the system (2.1) by $\mathbf{l}_j$, $j = 1, ..., n$.

There are cases where the set of O.D.E's given by (2.2) is integrable (the equations describing isentropic 1-D gas dynamic flows is such an example), hence the following holds:

$$\mathbf{l}_j \cdot \left(\frac{\mathrm{d}U}{\mathrm{d}t}\right)_j = \left(\frac{\mathrm{d}R_j}{\mathrm{d}t}\right)_j = 0, \quad j = 1, ..., n. \tag{2.4}$$

The functions R_j, $j = 1, ..., n$, which are defined by the above relation, are called *Riemann Invariants*, and they remain constant along the corresponding characteristic directions:

$$\frac{\mathrm{d}x}{\mathrm{d}t} = \lambda_j \quad j = 1, ..., n\,. \tag{2.5}$$

In general the system (2.2) is not integrable. Nevertheless, numerical evidence (coming mainly from results based on shock-capturing schemes for the 1-D Euler equations of gas dynamics, *e.g.* van Leer (1979), and Colella & Woodward (1984)) has shown that it is useful for numerical purposes to try to decompose the initial system of P.D.E's (2.1) to the set of O.D.E's (2.2) that hold along the characteristic curves, defined by (2.5); where the term *numerical purposes* should be interpreted as: "in order to develop algorithms that are both accurate and stable".

The case of non-homogeneous systems, *i.e.*

$$\frac{\partial U}{\partial t} + \frac{\partial F(U)}{\partial x} = G(U)\,, \tag{2.6}$$

is not so straightforward. Now the set of equations (2.2) does not hold along the characteristic curves (2.5). It should be useful, however, to see along which curves these equations hold. A straight forward calculation shows that along the trajectories defined by

$$\frac{\mathrm{d}x}{\mathrm{d}t} = \lambda_j - \frac{\mathbf{l}_j \cdot G(U)}{\mathbf{l}_j \cdot \partial U/\partial x} \quad j = 1, ..., n. \tag{2.7}$$

the set of O.D.E's (2.2) holds, and can be discretized and solved numerically, in the upwinding step of a shock capturing solver. This decomposition, of course, holds at smooth parts of the flow only, but this is not really a serious restriction.

Remember that the characteristic decomposition holds only when the solution is continuous, *i.e.* in the absence of shocks, but it is still used in a useful way when shocks are present because it holds on either side of the discontinuity. The situation is completely analogous for the decomposition defined by (2.2), (2.7). Also note that the computation of these curves can be performed at no extra cost, since the information about the spatial derivatives of the flow is always available at the points where the solution is known.

2.2 Mathematical Formulation of the 1-D Detonation Problem.

Consider a simple model of chemical interaction of two calorically perfect gases, $A \rightarrow B$, assuming one-step, irreversible, Arrhenius kinetics, and absence of dissipation mechanisms.

The conservation equations are given by:

$$\frac{\partial}{\partial t}\rho + \frac{\partial}{\partial x}(\rho u) = 0 \tag{2.8a}$$

$$\frac{\partial}{\partial t}(\rho u) + \frac{\partial}{\partial x}(\rho u^2 + p) = 0 \tag{2.8b}$$

$$\frac{\partial}{\partial t}(\rho e_t) + \frac{\partial}{\partial x}[(\rho e_t + p)u] = 0 \tag{2.8c}$$

$$\frac{\partial}{\partial t}(\rho z) + \frac{\partial}{\partial x}(\rho u z) = \rho g(T, z) \tag{2.8d}$$

with the total specific energy and the source term given by

$$e_t \equiv \frac{p}{\rho(\gamma - 1)} + q_0 z + \frac{u^2}{2}\ , \tag{2.9a}$$

$$g(T, z) = -K\, z \exp(-E_a/T)\ , \tag{2.9b}$$

and an equation of state given by

$$T = p/\rho\ . \tag{2.10}$$

In these equations, z is reactant mass fraction, γ, the specific-heat ratio, assumed common for both species, q_0 is the heat release parameter. E_a is the one-step chemical-reaction activation energy, and K is an amplitude parameter that sets the spatial and temporal scales. It should be mentioned that z takes values from the interval $[0,1]$. When the material is totally unreacted, then $z = 1$; when the reaction has been completed then $z = 0$.

Despite the simplicity of this model, computing such flows is quite challenging because for a wide range of values of the parameters of the reaction-rate equation, q_0 , E_a , K, the system of conservation laws is linearly and non-linearly unstable, and because the reaction-rate equation is generally very stiff and that leads to an extremely large range of (coupled) spatial and temporal modes. Required resolution for numerical simulation of these flows typically exceeds available computational resources.

The system (2.8) can be written in conservation form, *i.e.* in the form of (2.6) by setting

$$\begin{aligned} U &\equiv (u_1, u_2, u_3, u_4) = (\rho, \rho u, \rho e_t, \rho z)^T \\ F(U) &\equiv \left(u_2,\ u_2^2/u_1 + p(U),\ u_2/u_1(u_3 + p(U)),\ u_2 u_4/u_1\right)^T \\ G(U) &\equiv (0,\ 0,\ -q_0(\gamma-1)g(U),\ g(U))^T \ . \end{aligned} \tag{2.11}$$

with

$$\begin{aligned} p(U) &= (\gamma-1)(u_3 - 0.5u_2^2/u_1 - q_0 u_4)\ , \\ g(U) &= -K u_4\, exp(-E_a u_1/p(U))\ . \end{aligned} \tag{2.12}$$

The eigenvalues of the system are:

$$\begin{aligned} \lambda_1 &= u + \sqrt{\frac{\gamma p}{\rho}}\ , \\ \lambda_{2,3} &= u\ , \\ \lambda_4 &= u - \sqrt{\frac{\gamma p}{\rho}}\ . \end{aligned} \tag{2.13}$$

The result of the degeneracy of the second eigenvalue is that z can sustain jumps only across contact discontinuities.

Performing the decomposition of the system to a set of O.D.E's, as described in the previous subsection, one can define the following trajectories in the (x,t) plane:

$$\begin{aligned} \mathcal{C}_{\pm}: &\quad \frac{\mathrm{d}x}{\mathrm{d}t} = u \pm a + v_{\pm}, \\ \mathcal{C}_{0}: &\quad \frac{\mathrm{d}x}{\mathrm{d}t} = u + v_{0}, \\ \mathcal{C}_{\mathcal{R}}: &\quad \frac{\mathrm{d}x}{\mathrm{d}t} = u + v_{\mathrm{r}} \end{aligned} \tag{2.14}$$

with,

$$a \equiv \sqrt{\frac{\gamma p}{\rho}}$$

and,

$$\begin{aligned} v_{\pm} &\equiv -\frac{K\, q_0(\gamma-1)\,\rho z\, \exp(-E_a/T)}{\partial p/\partial x \;\pm\; \rho a\,(\partial u/\partial x)} \\ v_{0} &\equiv -\frac{K\, q_0(\gamma-1)\,\rho z\, \exp(-E_a/T)}{\partial p/\partial x \;-\; a^2\,(\partial \rho/\partial x)} \\ v_{\mathrm{r}} &\equiv \frac{K\, z\, \exp(-E_a/T)}{\partial z/\partial x} \end{aligned} \tag{2.15}$$

The scalar fields that hold along these trajectories are:

$$\begin{aligned} &\text{Along } \mathcal{C}_{\pm}: \quad \mathrm{d}p \pm \rho a\, \mathrm{d}u = 0, \\ &\text{Along } \mathcal{C}_{0}: \quad \mathrm{d}p - a^2\, \mathrm{d}\rho = 0 \\ &\text{Along } \mathcal{C}_{\mathcal{R}}: \quad \mathrm{d}z = 0. \end{aligned} \tag{2.16}$$

Note that, depending on the sign of the quantities defined by (2.15), the curves introduced above can be space-like or time-like.

2.3 Description of the numerical scheme.

To solve the system of equations (2.8) numerically a 2^{nd} order accurate MUSCL sheme is used. Consider a finite-volume formulation, *i.e.* space is discretized to a set of computational cells of length Δx. Additionally, consider mass-averaged values of the conservative variables

$$\begin{aligned} m_j &\equiv \int_{x_{j-1/2}}^{x_{j+1/2}} \rho dx \,, \\ m_j u_j &\equiv \int_{x_{j-1/2}}^{x_{j+1/2}} \rho u dx \,, \\ m_j e_{tj} &\equiv \int_{x_{j-1/2}}^{x_{j+1/2}} \rho e_t dx \,, \\ m_j z_j &\equiv \int_{x_{j-1/2}}^{x_{j+1/2}} \rho z dx \,. \end{aligned} \tag{2.17}$$

Finally, set

$$m_j g_j \equiv \int_{x_{j-1/2}}^{x_{j+1/2}} \rho g(T,z) dx \,.$$

In the above expressions, average values of all quantities in the j^{th} cell are denoted by the subscript j, while values of various quantities at the cell boundaries are denoted by $j \pm 1/2$. By setting

$$\begin{aligned} F_m &\equiv \rho u \,, \\ F_u &\equiv \rho u^2 + p \,, \\ F_e &\equiv \rho e_t u + p u \,, \\ F_z &\equiv \rho z u \,. \end{aligned} \tag{2.18}$$

the conservation equations are now written for the j^{th} cell

$$\begin{aligned} \frac{dm_j}{dt} + (F_m)_{j+1/2} - (F_m)_{j-1/2} &= 0 \,, \\ \frac{d}{dt}(m_j u_j) + (F_u)_{j+1/2} - (F_u)_{j-1/2} &= 0 \,, \\ \frac{d}{dt}(m_j e_{tj}) + (F_e)_{j+1/2} - (F_e)_{j-1/2} &= 0 \,, \\ \frac{d}{dt}(m_j z_j) + (F_z)_{j+1/2} - (F_z)_{j-1/2} &= m_j g_j \,. \end{aligned}$$

As in the case of the scalar conservation law, we assume linear interpolation of all quantities at each cell, and slopes given by van Leer's limiter (1.15). The proposed scheme, giving the solution at time $(n+1)\Delta t$ from the solution at the previous time $n\Delta t$ can be written as:

$$
\begin{aligned}
(m_j)^{n+1} &= (m_j)^n - \Delta t \left[(F_m)^{n+1/2}_{j+1/2} - (F_m)^{n+1/2}_{j-1/2} \right] , \\
(m_j u_j)^{n+1} &= (m_j u_j)^n - \Delta t \left[(F_u)^{n+1/2}_{j+1/2} - (F_u)^{n+1/2}_{j-1/2} \right] , \\
(m_j e_{tj})^{n+1} &= (m_j e_{tj})^n - \Delta t \left[(F_e)^{n+1/2}_{j+1/2} - (F_e)^{n+1/2}_{j-1/2} \right] , \\
(m_j z_j)^{n+1} &= (m_j z_j)^n - \Delta t \left[(F_z)^{n+1/2}_{j+1/2} - (F_z)^{n+1/2}_{j-1/2} \right] + \Delta t \, (m_j g_j)^{n+1/2} ,
\end{aligned}
\tag{2.19}
$$

where the numerical fluxes $(F_m)^{n+1/2}_{j+1/2}$, $(F_u)^{n+1/2}_{j+1/2}$, $(F_e)^{n+1/2}_{j+1/2}$, $(F_z)^{n+1/2}_{j+1/2}$ are given by equations (2.17), solving the set of O.D.E's (2.15) numerically along the trajectories defined by (2.14). The case where a denominator in (2.15) (*i.e.* the expressions for u_+, u_-, u_0, u_r) vanishes, is treated in the same way as in the scalar law. Since the points of vanishing denominators are not points of singularity but simply points of zero convection locally, the necessary information for upwinding can be obtained by Taylor expansion in time. This procedure ensures uniformly 2^{nd} degree of accuracy in both space and time for smooth parts of the flow.

Of cource the above set of O.D.E's has to be supplemented with the appropriate jump relations, in order to take care of the presence of the discontinuities, *i.e.* a Riemann Problem has to be solved locally at each cell interface *. This procedure guarantees 2^{nd} order accuracy uniformly in space and time. The solution of the Riemann problem corresponding to this set of equations, dubbed as "Generalized Riemann Problem" (GRP), is not the same as the solution to the classical 1-D gas-dynamic Riemann Problem (RP). The GRP is not a self-similar problem and

* The jump relations have to be used in the cells where the density and pressure slopes are large. These are identified as the *critical* cells, since a nonlinear wave pattern might emerge in these cells in finite time. A detailed description of the Riemann solver that was used can be found in Lappas *et al.* (1993).

its solution is more complicated. The shock and expansion waves are curved in the (x,t) plane; *i.e.* they are accelerating. The solution to the GRP has been worked out by Ben-Artzi (1989). It is shown that the solution approaches the solution of the RP in the limit $x \to 0$, $t \to 0$, hence the solution to the RP can be used for numerical purposes. It will be shown later that, using this approximation, the acceleration of the various ways can be captured numerically quite well.

2.4 Numerical Results for 1-D Detonations.

In the early 40's Zeldovich, von Neumann, and Doering independently proposed that detonations waves in one-dimensional flows are steady shock waves propagating in a medium of local thermodynamic equilibrium, followed by a reaction zone of finite length. This theory is known historically as the ZND theory of detonations. Given a fixed state ahead of the detonation, the computation of the spatial profiles of the solution redusces to the numerical integration of a nonlinear ODE, see *e.g.* Fickett and Davis (1979). Typical spatial ZND profiles for pressure and reactant mass fraction are given in Figs. 10.

For detonations governed by the one-step irreversible Arrhenius law (2.9*b*) there is a minimum shock velocity, and that is the Chapman-Jouguet velocity, D_{CJ}. A reaction process characterized by this shock speed is called Chapman-Jouguet detonation. The point at the end of the reaction zone of a Chapman-Jouguet detonation is sonic. For every detonation the wave speed, D, has to satisfy $D \geq D_{CJ}$. The parameter f, defined as

$$f \equiv \left(\frac{D}{D_{CJ}}\right)^2 ,$$

is the overdrive factor of the detonation. In particular, by fixing the values of the parameters γ, q_0, and E_a, there is an one-on-one correspondence between the overdrive factor, f, and the stiffness parameter, K. The overdrive factor decreases as the stiffness of the reaction-rate equation, K, increases; *i.e.* the faster the reaction, the lower the overdrive. The half-reaction length, $L_{1/2}$, that is the distance between the shock wave and the point where $z = 0.5$, will be used as unit length throughout.

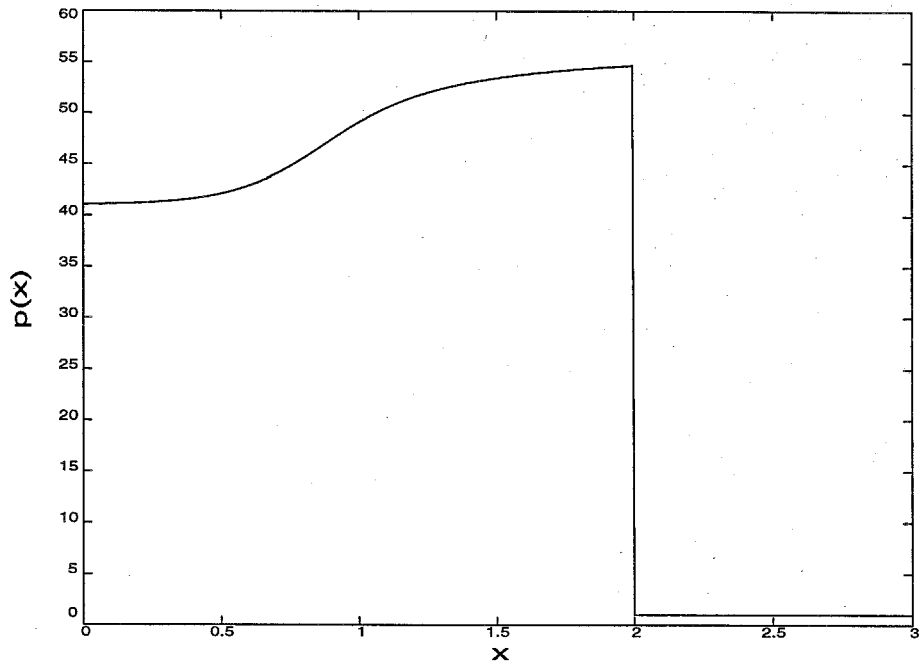

FIG. 10a Typical spatial profile of pressure for a ZND detonation.

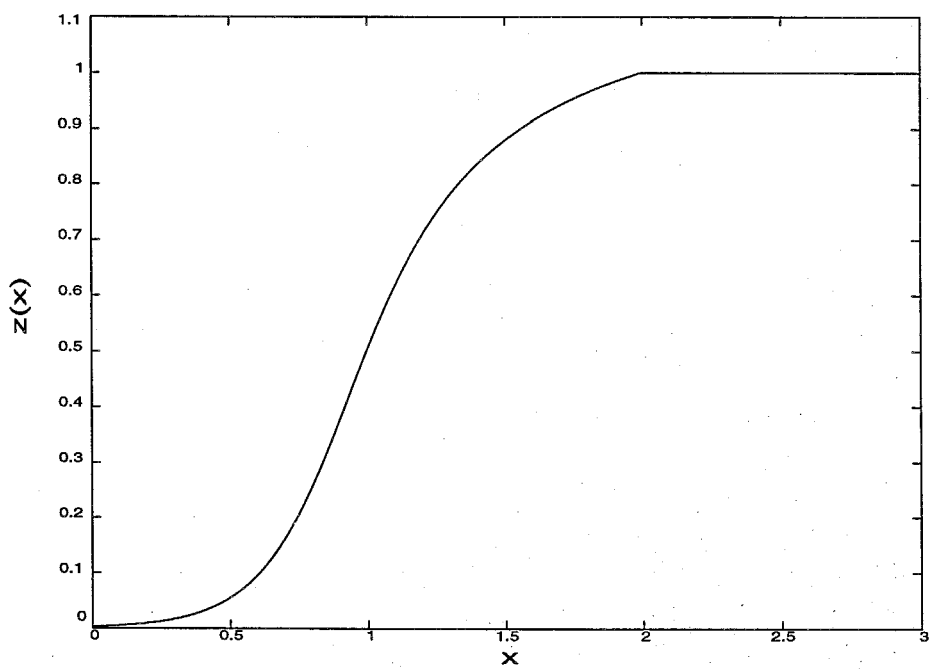

FIG. 10b Typical spatial profile of reactant mass fraction for a ZND detonation.

Experimental studies suggest, in contrast with the ZND theory, that detonation phenomena are generally unstable and possess a far more complicated structure than the one predicted by the ZND theory, see *e.g.* Fickett and Davis (1979). Linear stability analysis of the conservation equations (2.8), (2.9), by Erpenbeck (1964), and Lee & Stewart (1991) verify that for a large range of values of the parameters γ, q_0, E_a, and K, the system is unstable.

In the following, the variables and the parameters of the system have been made dimensionless by reference to the constant state ahead of the detonation front, hence $f(K)$ has become the stability parameter of the system. The remaining parameters have been fixed as follows:

$$\gamma = 1.2, \quad q_0 = 50, \quad E_a = 50.$$

According to the afore-mentioned stability studies there is a critical value f^* at which the real part of one of the eigenmodes of the system changes sign and becomes positive. For overdrives below that critical value, the system is unstable, with more and more eigenmodes becoming unstable as f decreases. This critical value is $f^* = 1.72$.

In the numerical simulations presented here, the spatial ZND profiles for various overdrive factors are evaluated, and given to the computer code as initial data. The truncation error is left to trigger the instabilities, and the whole evolution process is observed. The state at the left boundary is always given by the state at the end of the reaction zone at $t = 0$, that is the left end-point of the ZND profile. All computations were performed with a modified CFL number

$$\frac{\Delta t}{\Delta x} \, |v|_{\max} = 0.5 \, ,$$

where $|v|_{\max} \equiv \max\{|u+a+v_+|, \; |u+a+v_-|, \; |u+v_0|, \; |u+v_r|\}$, except in the cases where a denominator in (2.15) vanished. As mentioned earlier, Taylor expansion in time was used for these isolated cases.

As a first test, the overdrive factor was taken to be $f = 1.8$. This is the case of a stable detonation. The shock speed and stiffness coefficient, for that overdrive,

are $D = 9.1357$, and $K = 145.69$, respectively. The time history of the shock pressure (*i.e.* the pressure immediately behind the shock) is presented in Fig. 11; the fluctuation of the shock pressure decays with time. The resolution for that simulation was $15\,\text{pts.}/L_{1/2}$. The results of the time history of the shock pressure are in very good agreement with the results obtained by Bourlioux *et al.* (1991), using the PPM algorithm and front tracking, with the same resolution.

Next, the overdrive factor was lowered to $f = 1.6$, which corresponds to $D = 8.6134$, and $K = 230.75$. Linear stability analysis predicts one unstable mode for this case. The time history of the shock pressure is presented in Fig. 12a. Spatial profile of pressure at time $t = 80.0$ is presented in Fig. 12b. Following Quirk (1993), a convergence study for the peak shock pressure for various numerical schemes was performed, and the results are presented in Fig. 12c. The numerical schemes are: PPM with front tracking and mesh refinement (Bourlioux *et al.* (1991)), Roe's solver with Superbee Limiter (Quirk (1993)), Roe's Solver with the Minmod Limiter (Quirk (1993)), and the present unsplit scheme. In that figure a relative mesh spacing of 1 correspnds to a resolution of $10\,\text{pts.}/L_{1/2}$; similarly a relative mesh spacing of 0.25 corresponds to a resolution of $40\,\text{pts.}/L_{1/2}$. Note that the schemes converge to the result given by Fickett and Wood (1966), who estimated the peak pressure at the value of 98.6.

Subsequently numerical results were obtained for the cases of overdrive factor $f = 1.40$ and $f = 1.34$. For $f = 1.40$ the parameters are $D = 8.06$, and $K = 411.98$. Linear stability analysis predicts two unstable modes. The shock pressure history, which exhibits a period-doubling oscillation, is presented in Fig. 13a, and the spatial profile of pressure at time $t = 100$ is presented in Fig. 13b. For $f = 1.34$ the parameters of the problem are $D = 7.88$ and $K = 504.91$. This is a case of three unstable modes according to linear stability analysis. The shock pressure history and the spatial profile of pressure at $t = 100$ are presented in Figs. 14. These results were obtained with a resolution of $40\,\text{pts.}/L_{1/2}$ for both overdrives. Numerical simulations with higher resolution produced the same results in both cases.

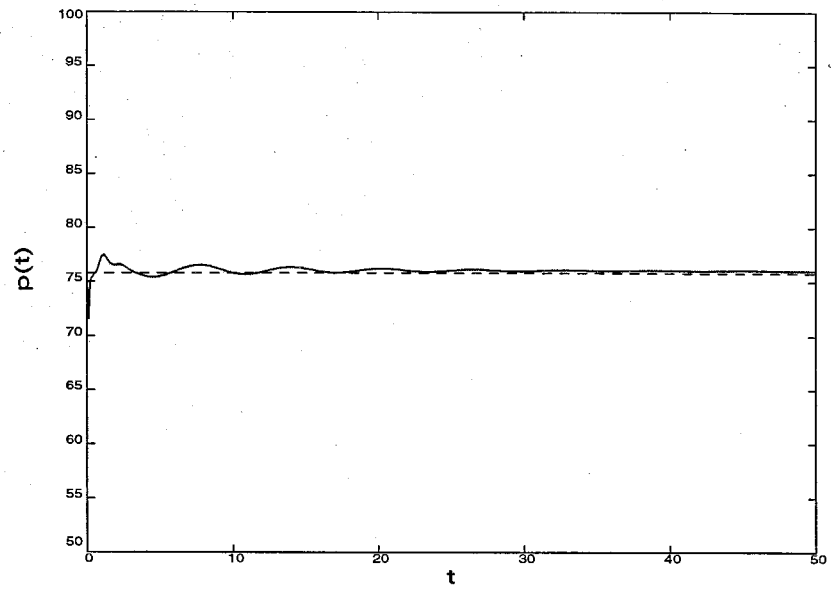

FIG. 11 Time history of the shock pressure for a ZND detonation of overdrive factor $f = 1.80$. Resolution 15 pts./$L_{1/2}$. The horizontal line represents the ZND solution.

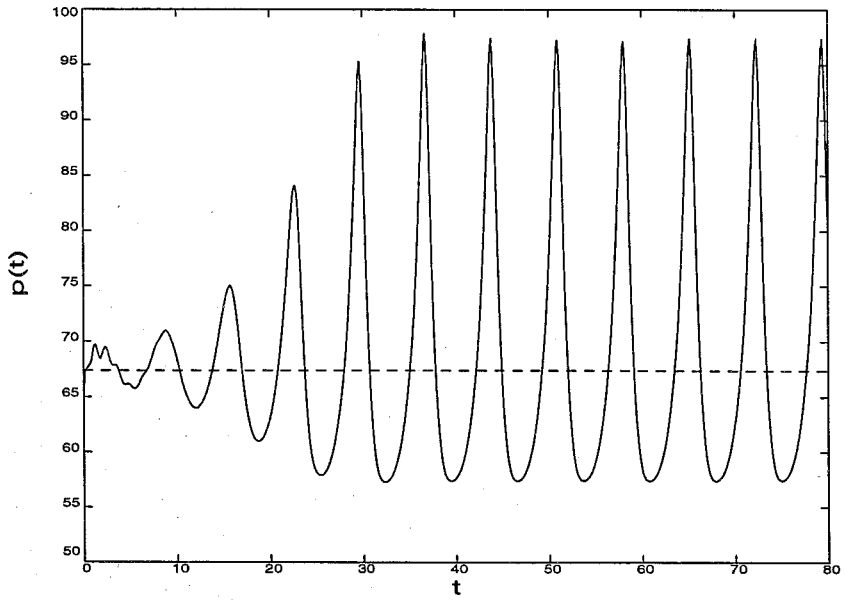

FIG. 12a Time history of the shock pressure for a ZND detonation of overdrive factor $f = 1.60$. Resolution 20 pts./$L_{1/2}$. The horizontal line represents the ZND solution.

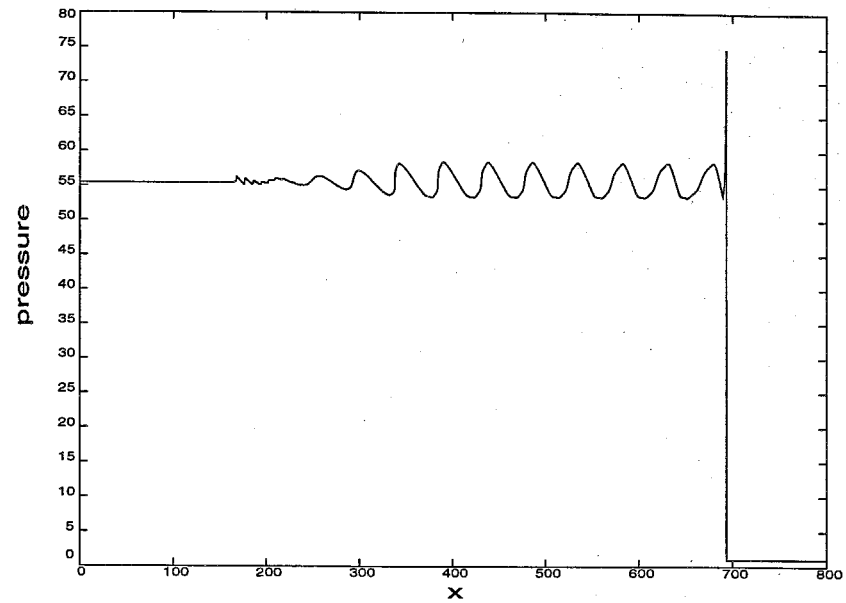

FIG. 12b Spatial profile of pressure for the ZND detonation of overdrive factor $f = 1.60$, at time $t = 80$. Resolution 20 pts./$L_{1/2}$.

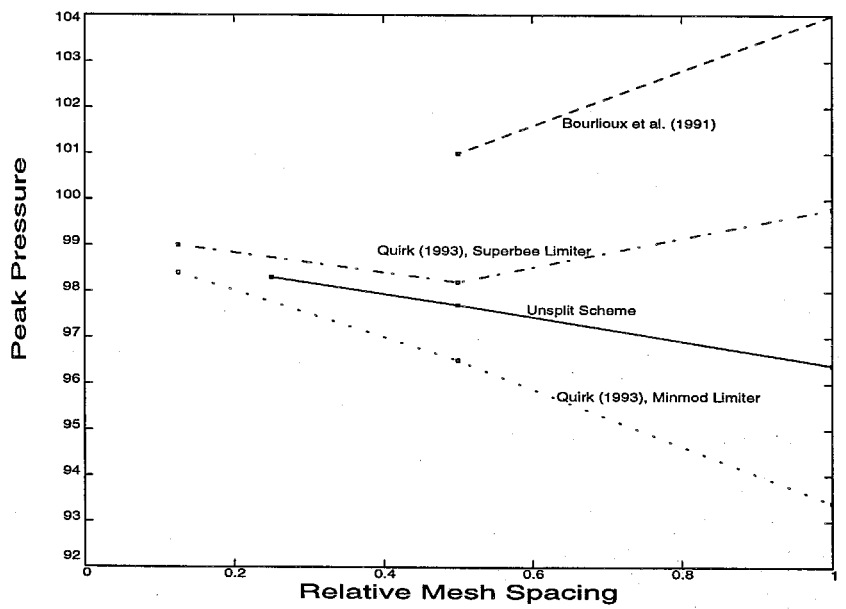

FIG. 12c Variation of peak pressure with grid resolution for various schemes. ZND detonation, overdrive factor $f = 1.60$.

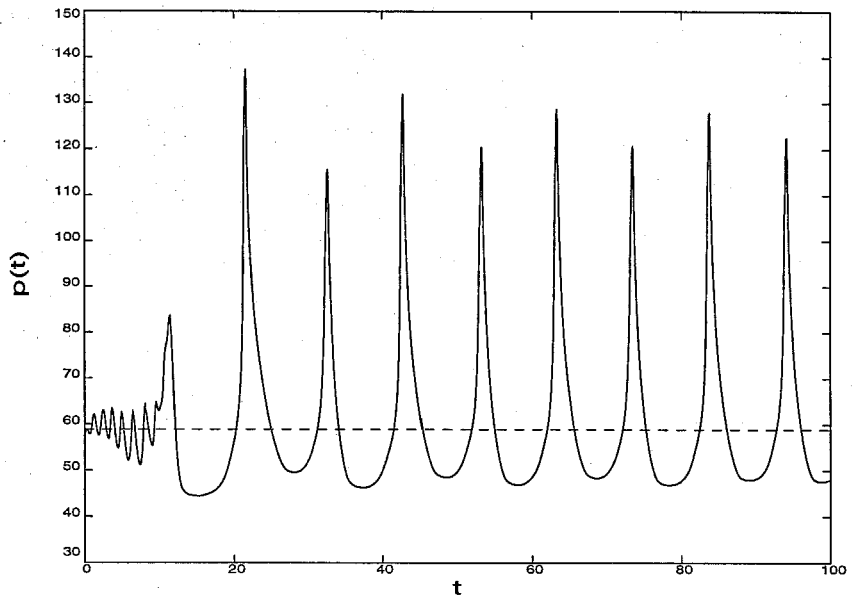

FIG. 13a Time history of the shock pressure for a ZND detonation of overdrive factor $f = 1.40$. Resolution 20 pts./$L_{1/2}$. The horizontal line represents the ZND solution.

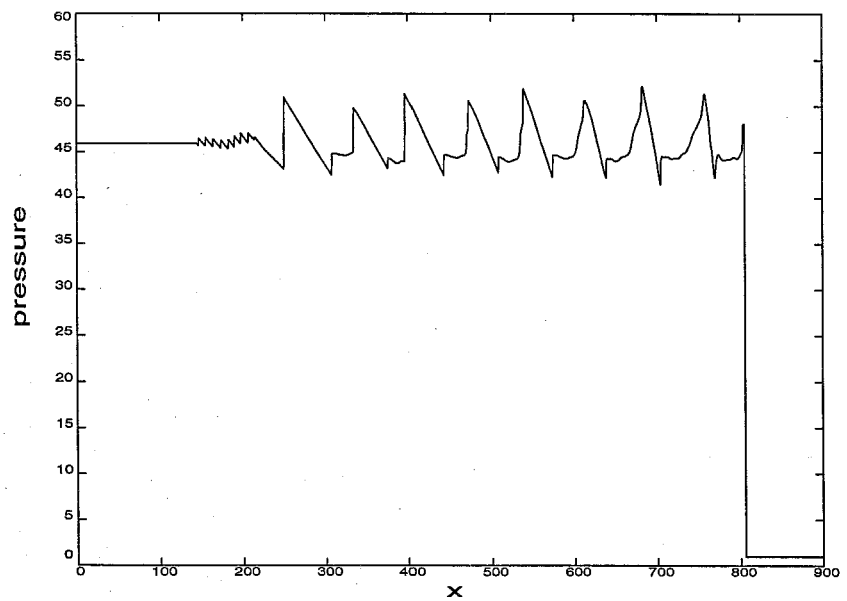

FIG. 13b Spatial profile of pressure for the ZND detonation of overdrive factor $f = 1.40$, at time $t = 100$. Resolution 20 pts./$L_{1/2}$.

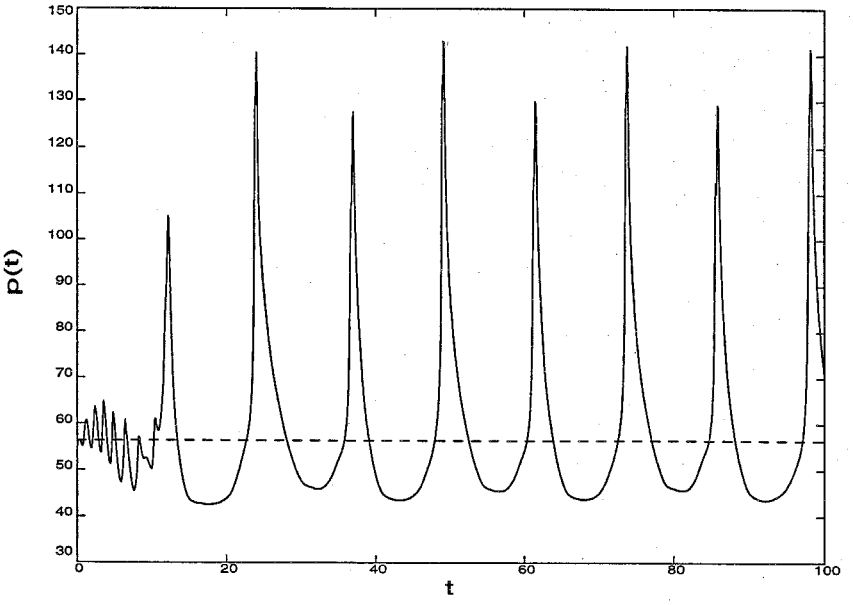

FIG. 14a Time history of the shock pressure for a ZND detonation of overdrive factor $f = 1.34$. Resolution 20 pts./$L_{1/2}$. The horizontal line represents the ZND solution.

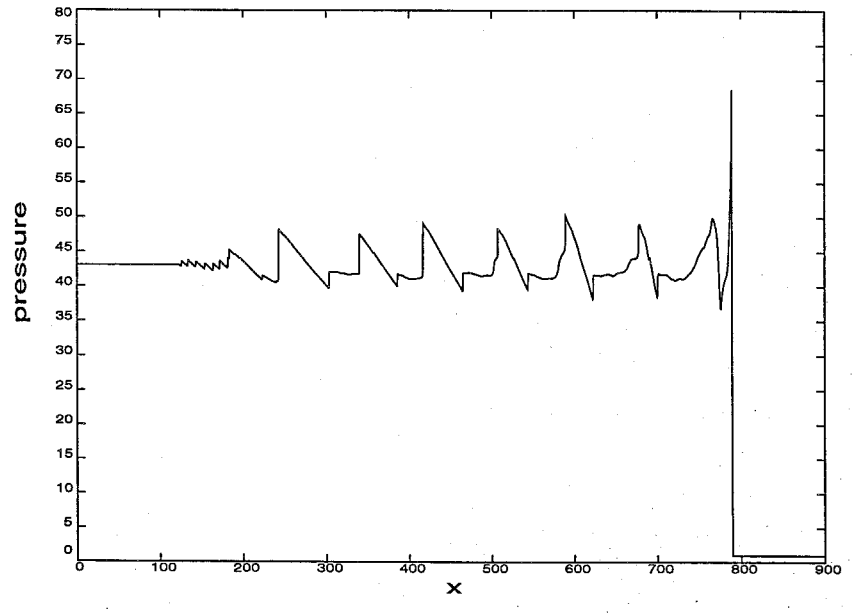

FIG. 14b Spatial profile of pressure for the ZND detonation of overdrive factor $f = 1.34$, at time $t = 100$. Resolution 20 pts./$L_{1/2}$.

Next, the overdrive factor was lowered even more, to a value of $f = 1.30$. The shock speed and the stiffness coefficient for this detonation are $D = 7.764$, and $K = 583.71$. Linear stability analysis suggests three unstable modes. Bourlioux *et al.* (1991), proposed the existence of chaotic pulsation instabilities because they observed a very sensitive dependence of the results on the initial data; slightly perturbed initial data produced results qualitatively similar but quantitatively different. Similar behavior was demonstrated in the present study by the simulations performed with the unsplit scheme. This can be verified by comparing the shock pressure history of unperturbed initial profiles as presented in Fig. 15a, with the pressure history of perturbed initial profiles in Fig. 15b. The perturbation that was added to the initial ZND profiles of the fluid dynamic variables was a sinusoidal wave of amplitude 0.1% of the values behind the shock wave. The wave length was taken equal to unity.

Numerical simulations using high-order algorithms for even lower overdrive factors had not been published until recently. Linear stability predicts an increased number of unstable modes as f decreases. He & Lee (1995) presented results obtained by a split algorithm, for overdrive factors as low as $f = 1.10$. For this case specifically, *i.e.* $f = 1.10$ which corresponds to shock speed $D = 7.1418$ and stiffness coefficient $K = 1389.58$, they found that the initial perturbations die out, that the post-shock values of the variables become steady, and that the reaction front stays behind the hydrodynamic shock at an ever increasing distance (quenched detonation). They explained this result by noticing that the first eigenmode of the system has become stable for this degree of overdrive. It should be emphasized, however that the other eigenmodes are still unstable, hence the system remains linearly unstable, let alone the fact that linear stability analysis is really helpful only for overdrives close to f^*, and not for overdrives close to unity.

Furthermore, this system of equations can not give a quenched detonation as a steady solution, even though it may indicate so for a short time. This is due to the phenomenon of thermal runaway: the reaction front stays temporarily behind the main shock, and the temperature in the area between the reaction front and the

shock is low. In this area, therefore, the source term on the right hand side of the species equation is exponentially small. The whole process in that region can be regarded as a homogeneous combustion, *i.e.* after some time the source term will become large and a rapid explosion will take place, resulting in tremendously high combustion spikes.

It is also worth noticing that temporal profiles in which the shock pressure drops to a steady value below the initial ZND value can be obtained for any unstable detonation which is underesolved, see *e.g.* underesolved results obtained in grid convergence studies by Bourlioux *et al.* (1991). In Fig. 16a an **underesolved** simulation for $f = 1.10$ is presented. The proposed unsplit scheme scheme was used and the resolution was $15\,\text{pts.}/L_{1/2}$. The result is in excellent agreement with the result of He & Lee (1995), obtained with a mesh of $50\,\text{pts.}/L_{1/2}$, up to time $t = 60.0$ (it is that time that He & Lee (1995) stoped their simulation). The very high increase in the shock pressure that occurs at time $t \simeq 65.0$ is due to the afore-mentioned phenomenon of thermal runaway.

When the resolution was increased in the current simulations, a dramatic change took place, see Fig. 16b. The temporal profile of the shock pressure became totally irregular, without any evident structure. It was observed that, at time $t \simeq 8.0$, the shock pressure drops to a value around $p \simeq 27.0$. The temperature at this point is around $T \simeq 3.4$ which is indeed too low to initiate the chemical reaction. Consequently the reaction front is just convected by the flow and stays behind the hydrodynamic shock.

In the region between the reaction front and the shock, however, the temperature is not constant. It can be verified that there are small pockets of material with higher temperature, see Fig. 17a. Recall that the initial fluctuations in the shock pressure produced shock waves that travelled upstream; these waves can be seen in Fig. 17. These waves interacted with each other and some reflected back, travelled downstream, and created the temperature gradients in the afore-mentioned region. The points of higher temperature are the points where the chemical reaction initi-

ates. The area between the initial reaction front and the hot spot remains inert. It will develop to a pocket of unreacted material as soon as the hot spot has burnt completely.

In the begining the reaction is slow because the source term in the species equation is still exponentially small. This early stage of the combustion can be considered a contant-pressure process. When the source term becomes larger, a relatively rapid explosion takes place. During this stage of the combustion the density is almost constant, therefore the temperature increase translates to a large pressure increase. This rise in pressure will result in a system with two shock waves, one travelling downstream and the other one upstream. The shock wave that propagates downstream will catch up the main shock. The time that this event takes place can be estimated by the shock pressure history *, Fig. 16b. The increase of the shock pressure will restart the detonation process behind the shock, until it drops again to a value $p \simeq 27.0$. The shock wave that propagates upstream will cause the explosion of the pocket of unreacted material. This second explosion gives birth to a second pair of shock waves. Spatial profiles of the flow variables during such an explosion are given in Figs. 18.

The whole process repeats itself until time $t \simeq 55$ when the explosions become very large. After that, the detonation oscillates in an irregular way, because of the presence of a large number of unstable modes in the system. For this case resolutions up to $250\,\text{pts.}/L_{1/2}$, were used. It was observed that different resolutions, finer than $15\,\text{pts.}/L_{1/2}$, produced qualitatively the same but quantitatively different results, at large times. It must be appreciated that for such a highly unstable case, different resolution essentially implies different initial data. Additional numerical investigations, with much higher resolutions, are definitely needed in order to achieve a final conclusion, but the numerical evidence obtained here clearly suggests that the detonation does not quench, and that the system exhibits chaotic behavior for $f = 1.10$.

---

* The sudden increases in the shock pressure at time up to $t \simeq 55$, correspond to the overtakings of the main front by the shocks that were produced during earlier explosions.

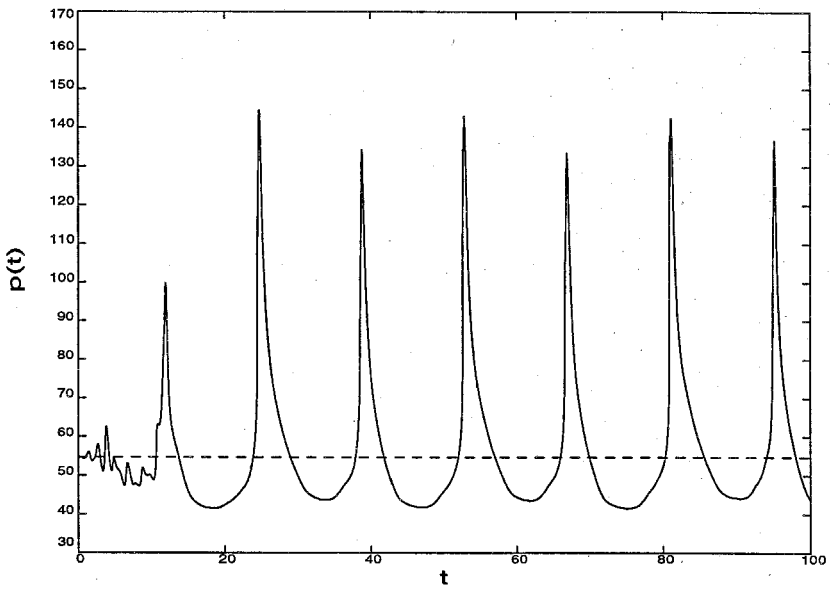

FIG. 15a Time history of the shock pressure for a ZND detonation of overdrive factor $f = 1.30$. Resolution 80 pts./$L_{1/2}$. The horizontal line represents the ZND solution.

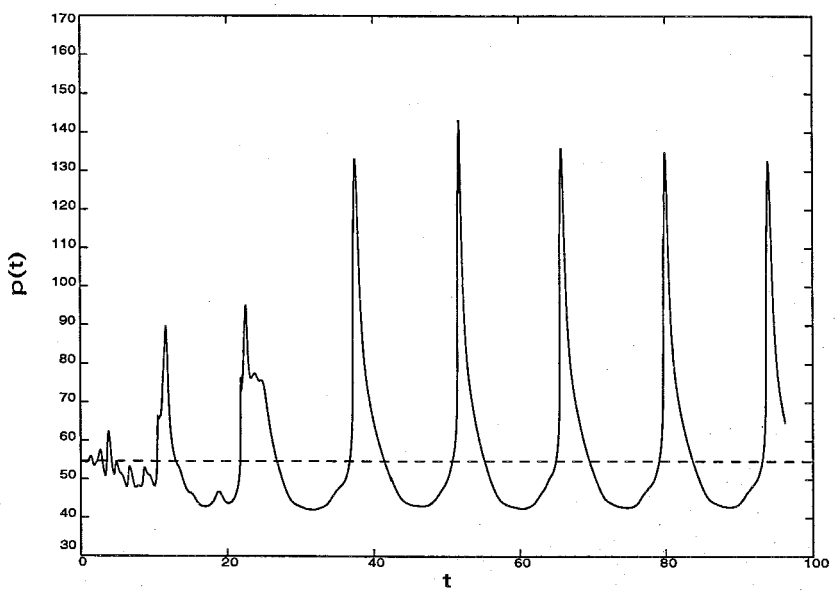

FIG. 15b Time history of the shock pressure for a ZND detonation of overdrive factor $f = 1.30$ with perturbed initial data. Resolution 80 pts./$L_{1/2}$. The horizontal line represents the ZND solution.

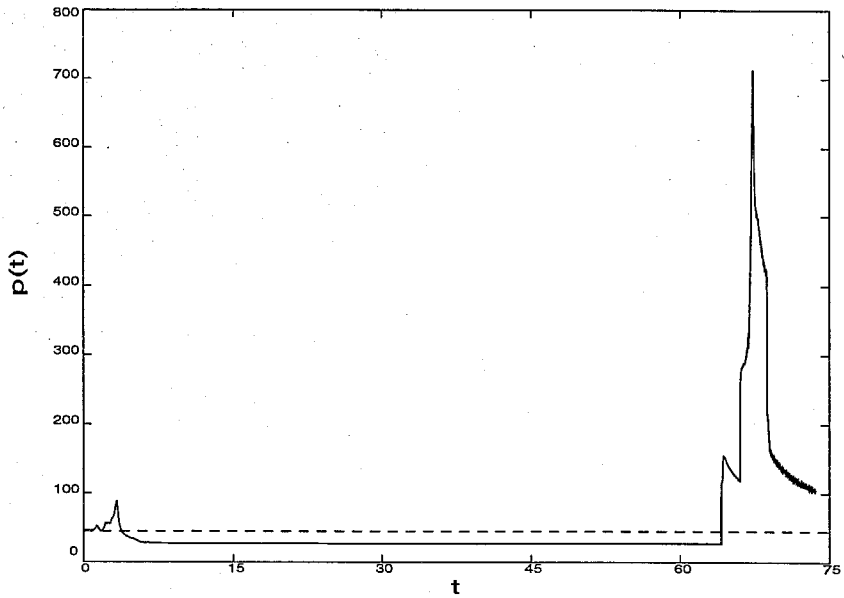

FIG. 16a Time history of the shock pressure for a ZND detonation of overdrive factor $f = 1.10$. Resolution 15 pts./$L_{1/2}$. The horizontal line represents the ZND solution.

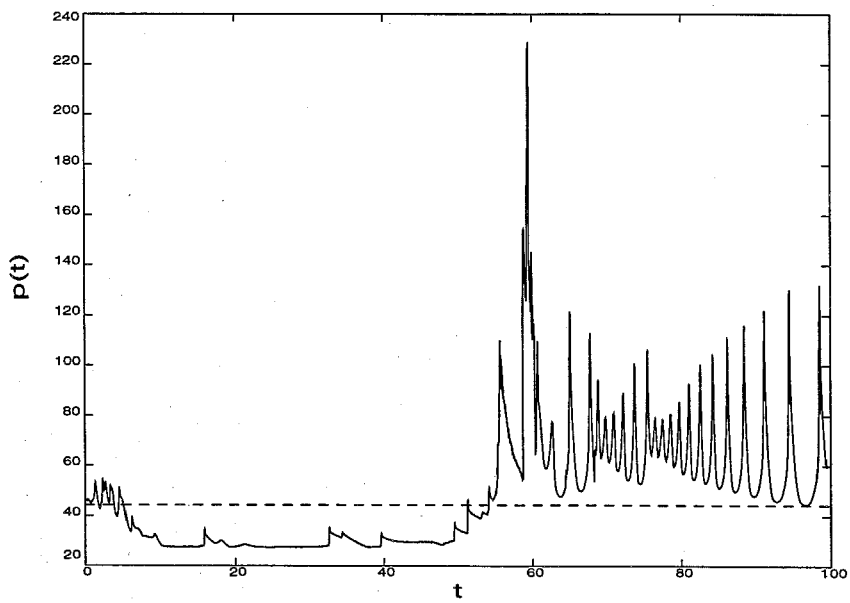

FIG. 16b Time history of the shock pressure for a ZND detonation of overdrive factor $f = 1.10$. Resolution 50 pts./$L_{1/2}$. The horizontal line represents the ZND solution.

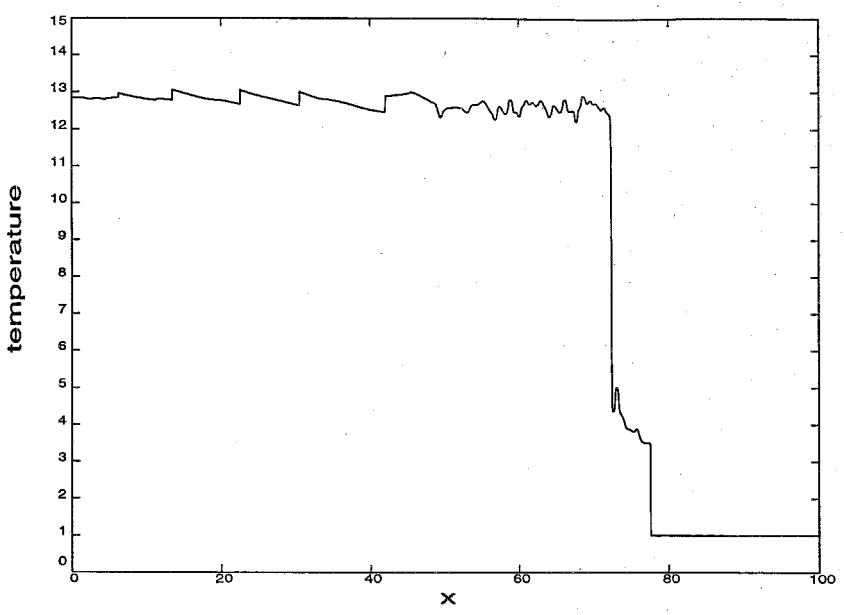

FIG. 17a Spatial profile of the temperature for the ZND detonation of overdrive factor $f = 1.10$, at time $t = 12.0$. Resolution 50 pts./$L_{1/2}$.

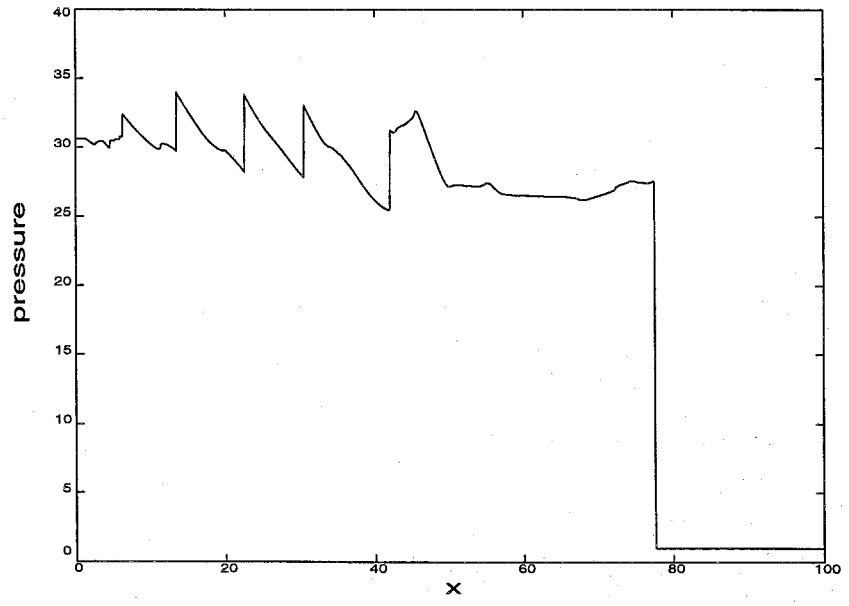

FIG. 17b Spatial profile of pressure for the ZND detonation of overdrive factor $f = 1.10$, at time $t = 12.0$. Resolution 50 pts./$L_{1/2}$.

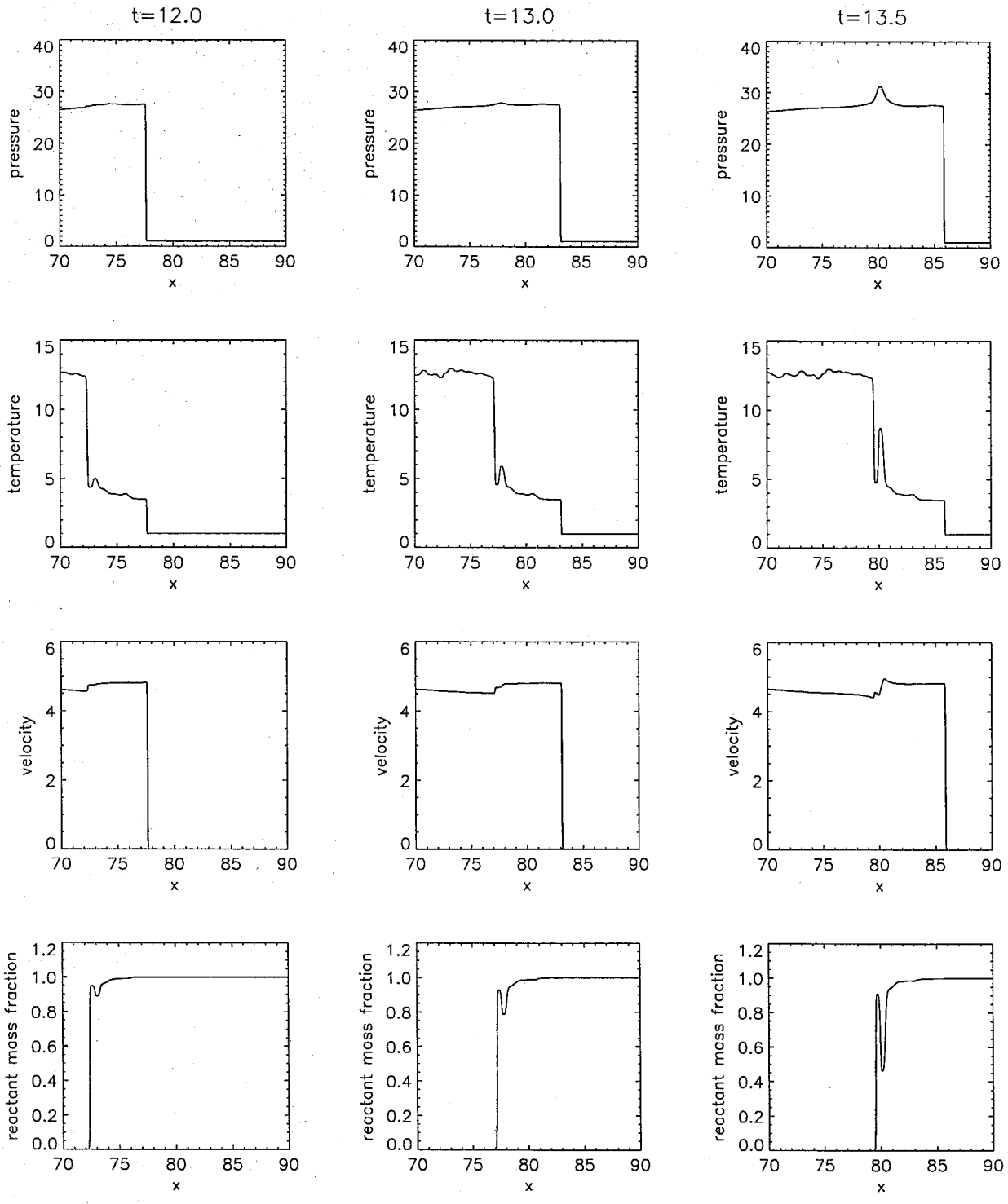

FIG. 18a Spatial profiles of the flow variables at the area of an explosion, for the ZND detonation of overdrive factor $f = 1.10$. Profiles taken at $t = 12.0, 13.0, 13.5$. Resolution 50 pts./$L_{1/2}$.

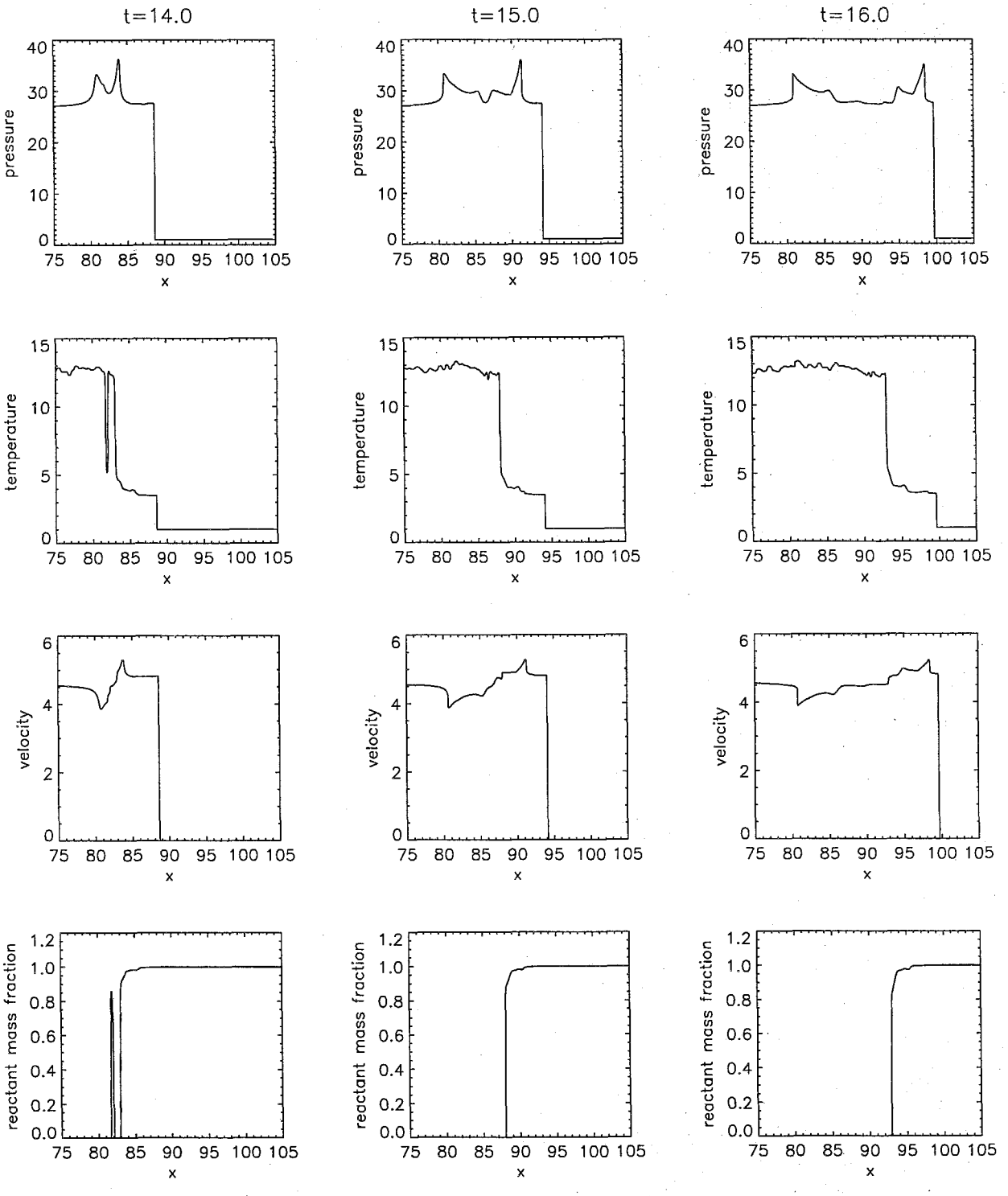

FIG. 18b Spatial profiles of the flow variables at the area of an explosion, for the ZND detonation of overdrive factor $f = 1.10$. Profiles taken at $t = 14.0, 15.0, 16.0$. Resolution 50 pts./$L_{1/2}$.

3. Concluding Remarks.

A new approach of looking at hyperbolic conservation laws has been presented. Performing the decomposition of the equations to a set of scalar fields along the proper trajectories in space-time, it is made possible to construct unsplit algorithm for the numerical integration of these laws. This approach can be regarded as a generalization of the method of characteristics.

The proposed scheme was tested on a scalar conservation law and on the one-dimensional Euler equations for reacting flows. The scheme is highly accurate and robust. In the scalar case increased stiffness may, depending on the data, produce smooth travelling wave solutions with very high velocities. Unless the computational grid is sufficiently resolved, these velocities can not be captured correctly with explicit schemes. This phenomenon is similar to the well known case of spurious shock wave speeds. With sufficient resolution the proposed unsplit scheme is considerably more accurate than the equivalent split version.

In the case of reacting flows, useful insight for the evolution of ZND detonations in the unstable regime was obtained. The question of the long time behavior of detonations near the CJ point is still open, but the results obtained by the present scheme clearly suggest a chaotic behavior of the system, in contrast with the prediction of He & Lee (1995).

An important advantage of the new approach is that it can be generalized to handle multidimensional flows, in a straightforward way. The system of conservations laws can be decomposed to a set of O.D.Es, similarly as in the 1-D case. But now these O.D.E's hold along manifolds in the (x, y, t) space. The study of the geometry of these manifolds and the design of unsplit multidimensional algorithms, is the subject of future work.

4. Acknowledgements

Effort sponsored by the Air Force Office of Scientific Research, under grant numbers F49620-94-1-0353 and F49626-93-1-00338. The US Government is authorized to reproduce and distribute reprints for Governmental purposes notwithstanding any copyright notation thereon.

References.

1. ABOUSEIF, G. and TOONG, T.Y., *Theory of unstable one-dimensional detonations*, Combust. Flame (1982), Vol. **45**, pp. 67-94.

2. BEN-ARTZI, M., *The generalized Riemann problem for reactive flows*, J. Comp. Phys. (1989), Vol. **81**, pp. 70-101.

3. BOURLIOUX, A., *Numerical study of unstable detonations*, Ph.D. Thesis, Princeton University, (1991).

4. BOURLIOUX, A., MAJDA, A.J., and ROYTBURD, V., *Theoretical and numerical structure for unstable one-dimensional detonations*, SIAM J. Appl. Math, (1991), Vol. **51**, pp. 303-343.

5. CHEN, G., LEVERMORE, C., and LIU, T.P., *Hyperbolic conservation laws with stiff relaxation terms and entropy*, Comm. Pure Appl. Math. (1994), Vol. **47**, pp. 787-830.

6. CHOI, Y.S., and MAJDA, A.J., *Amplification of small-amplitude high- frequency waves in a reactive mixture*, SIAM Review (1989), Vol. **31**, pp. 401-427.

7. COLELLA, P., MAJDA, A.J., and ROYTBURD, V., *Theoretical and numerical structure of reacting shock waves*, SIAM J. Sci. Stat. Comp. (1986), Vol. **7**, pp. 1059-1080.

8. COLELLA, P., and WOODWARD P.R., *The PPM method for gas dynamic simulations*, J. Comp. Phys. (1984), Vol. **54**, pp. 174-201.

9. COURANT, R., and HILBERT., D.,*Methods of mathematical physics, Vol. II*, Interscience, New York, (1963).

10. CRANDALL, M.G., and MAJDA, A.J., *Monotone differnce approximations for scalar conservation laws*, Math. Comp. (1980), Vol. **34**, pp. 1-21.

11. DI PERNA R.J., and MAJDA A.J., *The validity of nonlinear geometric optics for weak solutions of conservation laws*, Comm. Math. Phys. (1985), Vol. **98**, pp. 313-347.

12. DOERING, W., *On detonation processes in gases*, Ann. Phys. (1943), Vol. **43**, pp. 421-436.

13. ENGQUIST, B., and SJOGREEN, B., *Robust difference approximations of stiff inviscid detonation waves*, UCLA-CAM Report 91-03 (1991).

14. ERPENBECK, J.J., *Stability of idealized one-reaction detonations*, Phys. Fluids (1964), Vol. **7**, pp. 684-696.

15. FICKETT, W., and DAVIS, W.C., *Detonation*, U.C. Berkeley Press, (1979).

16. FICKETT, W., and WOOD, W.W., *Flow calculation for pulsating one- dimensional detonation*, Phys. Fluids (1966), Vol. **9**, pp. 903-916.

17. GRIFFITHS, D.F., STUART, A.M., and YEE, H.C., *numerical wave propagation in an advection equation with a nonlinear source term*, SIAM J. Numer. Anal. (1992), Vol. **29**, pp. 1244-1260.

18. HARTEN, A., ENGQUIST, B., OSHER, S., and CHAKRAVARTHY, S., *Uniformly high order accurate ENO schemes, III*, J. Comp. Phys. (1987), Vol. **71**, pp. 231-303.

19. HE, L.T., and LEE, J.H.S., *The dynamical limit of one-dimensional detonations*, Phys. Fluids (1995), Vol. **7**, No **5**, pp. 1151-1159.

20. KAPILA, A.K., MATKOWSKY, B.J., and VAN HARTEN A., *An asymptotic theory of deflagrations and detonations. I. The steady solutions.*, SIAM J. Appl. Math. (1983), Vol. **43**, pp. 491-519.

21. KRUZKOV, S.N., *First order quasilinear equations in several dependent variables*, Math. Sbornik (1970), Vol. **123**, pp. 217-243.

22. LAPPAS, T., LEONARD, A., and DIMOTAKIS, P.E., *An adaptive Lagrangian method for computing 1D reacting and non-reacting flows.* J. Comp. Phys. (1993), Vol. **104**, pp. 361-376.

23. LAPPAS, T., LEONARD, A., and DIMOTAKIS, P.E., *Riemann Inavariant Manifolds for the multidimensional Euler equations*, under review by the SIAM J. Sci. Comp. (1995).

24. LAX, P., *Hyperbolic systems of Conservation laws ane the mathematical theory of shock waves*, SIAM (1973).

25. LAX, P., *Hyperbolic systems of Conservation laws II.*. Comm. Pure Appl. Math. (1957), Vol. **10**, pp. 537-566.

26. LEE, H.I., and STEWART, D.S., *Calculation of linear detonation instability: one- dimensional instability of plane detonation*, J. Fluid. Mech. (1990), Vol. **206**, pp. 103-132.

27. LE VEQUE, R.J., and SHYUE, K.M., *One dimensional front tracking based on high resolution wave propagation mathods*, SIAM J. Sci. Comp. (1995), Vol. **16**, pp. 348-377.

28. LE VEQUE, R.J., *Numerical methods for conservation laws*, Birkhauser Verlag, Zurich, (1992).

29. LE VEQUE, R.J., and YEE, H.C., *A study of numerical methods for hyperbolic conservation laws with stiff source terms*, J. Comp. Phys. (1990), Vol. **86**, pp. 187-209.

30. LIONS, P.L., and SOUGANIDIS, P.E., *Convergence of MUSCL and filtered schemes for scalar conservation laws and Hamilton-Jacobi equations*, Math. Comp. (1995), Vol. **69**, pp. 441-470.

31. LIU, T.P, *Hyperbolic conservation laws with relaxation*, Comm. Math. Phys. (1987), Vol. **108**, pp. 153-175.

32. MAJDA A.J., and ROSALES R.R., *Resonantly interacting weakly nonlinear hyperbolic waves. I. A single space variable*, Studies Appl. Math. (1984), Vol. **71**, pp. 149-179.

33. MAJDA A.J., and ROSALES R.R., *Nonlinear mean field - high frequency wave interactions in the induction zone*, SIAM J. Appl. Math (1987), Vol. **47**, pp. 1017-1039.

34. MAJDA, A.J., and ROYTBURD, V., *Numerical study of the mechanisms for initiation of reacting shock waves*, SIAM J. Sci. Stat. Comp. (1990), Vol. **11**, pp. 950-974.

35. OSHER, S, and SETHIAN, J.A., *Fronts propagating with Curvature dependant speed: ALgorithms based on Hamilton-Jacobi Formulations*, J. Comp. Phys. (1988), Vol. **79**, pp. 12-49.

36. ORAN, E., and BORIS, J.P., *Numerical simulation of reactive flow*, Elsevier, New York, (1987).

37. PEMBER, R., *Numerical Methods for hyperbolic conservation laws with stiff relaxation I. spurious solutions*, SIAM J. Appl. Math. (1993), Vol. **53**, pp. 1293-1330.

38. ROE, P.H., *Approximate Riemann solvers, parameter vectore, and difference schemes*, J. Comp. Phys. (1981), Vol. **43**, pp. 357-372.

39. QUIRK, J.J., *Godunov-type schemes applied to detonation flows*, ICASE report No. 93-15, (1993).

40. SETHIAN, J.A., *Numerical algoithms for propagating interfaces: Hamilton- Jacobi equations and conservation laws*, J. Diff. Geometry (1990), Vol. **31**, pp. 131-161.

41. SMOLLER, J., *Shock waves and reaction-diffusion equations*, Springer-Verlag, New York, (1983).

42. STRANG, J., *On the construction and comparison of differnce schemes*, SIAM J. Num. Anal. (1968), Vol. **5**, pp. 506-517.

43. TANG, T, and TENG Z.H., *Error bounds for fractional step methods for conservation laws with source terms*, SIAM J. Num. Anal. (1995), Vol. **32**, pp. 110-127.

44. VAN LEER, B., *Towards the ultimate conservative difference scheme. IV. A new approach to numerical convection*, J. Comp. Phys. (1977), Vol. **23**, pp. 276-299.

45. VAN LEER, B., *Towards the ultimate conservative difference scheme. V. A second order sequel to Godunov's Method*, J. Comp. Phys. (1979), Vol. **32**, pp. 101-136.

46. VAN LEER, B., *On the relation between the upwind-differncing schemes of Godunov, Engquist-Osher and Roe*, SIAM J. Sci. Stat. Comput. (1984], Vol. **5**, pp. 1-20.

47. VON NEUMANN, J., *Theory of detonation waves*, John Von Neumann Collected works, Vol. 6, Macmillan, New York, (1942).

48. YEE, H.C., *A class of high-resolution explicit and implicit shock- capturing methods*, Von Karman Institue, Belgium (1987).

49. ZELDOVICH, Y.B., *On the theory of the propagation of detonation in gaseous systems*, (English Translation), NACA TM 1261 (1960).